Electronic Research Archive

https://www.aimspress.com/journal/era

ERA, 34(1): 376–410.
DOI: 10.3934/era.2026018
Received: 26 September 2025
Revised: 28 November 2025
Accepted: 25 December 2025
Published: 14 January 2026

Research article

Stochastic modeling of intimacy-conflict dynamics in non-traditional stable marriages

Xinying Liu[1,2,*]

[1] College of Media Engineering, Communication University of Zhejiang, Hangzhou 310018, China
[2] Zhejiang Key Laboratory of Film and TV Media Technology, Hangzhou 310018, China

* **Correspondence:** Email: xinying@cuz.edu.cn.

Abstract: Most prior couple dynamics research has focused on either high-conflict, low-stability relationships or low-conflict, high-stability relationships, relying predominantly on deterministic models. We investigate the stability of the far-less-studied dynamically balanced regime characterized by recurrent small conflicts, occasional large conflicts, and spontaneous repair processes in an intrinsically stochastic environment. An intimacy–conflict model couples dual stochasticity: event timing follows independent Poisson processes, and impact magnitudes follow uniform distributions. Formal proofs establish the existence and uniqueness of solutions, bounded states within [0, 1], stochastic stability of intimacy around its baseline, and convergence to a unique stationary distribution. Simulations show that intimacy drifts back to its usual level, that the impact of each event depends on the couple's current state, and that built-in repair keeps the system steady while mirroring real-life ups and downs. The study extends theory on conflict–intimacy coevolution and provides a framework for marital research and intervention.

Keywords: marital relationship mode; stochastic differential equations; stochastic stability; sensitivity analysis

1. Introduction

Marital relationships, as foundational units of social networks, play a crucial role in the stability of family systems and are closely linked to individuals' mental health, physical well-being, and overall life satisfaction [1]. While previous studies have identified a range of marital interaction patterns, most research has focused on two primary prototypes: the traditionally stable low-conflict–high-intimacy type and the less stable high-conflict–low-intimacy type. However, a distinct pattern—which we term the *dynamically balanced* marital pattern, that is, long-term unions that simultaneously exhibit high conflict frequency, high intimacy, and high subjective well-being, representing approximately 15–25% of couples [2–5]—which combines high-frequency conflicts with long-term relationship stability has

received insufficient attention.

This study identifies a unique phenomenon in long-term cohabitation: a cyclical and hierarchical distribution of conflicts characterized by frequent small conflicts and occasional large conflicts accompanied by intense emotional exchanges. Crucially, this pattern relies on *endogenous repair* mechanisms—spontaneous positive interactions initiated by the partners themselves, such as unplanned small gifts or emotional expressions, without external intervention or scheduled therapy [6, 7]—rather than external interventions. These hierarchical conflicts include high-frequency and low-intensity disputes that arise over household chores and involve short recovery cycles as well as low-frequency and high-intensity disagreements rooted in value differences and not leading to separation behaviors. While such conflicts have been qualitatively observed, existing classifications lack quantitative rigor, as they lack objective thresholds to distinguish intensity or duration and do not provide probabilistic characterization of temporal patterns. These shortcomings limit the modeling of their non-deterministic yet statistically predictable dynamics.

Despite ongoing high-frequency conflicts, these couples remain together, share family responsibilities, and notably exhibit advantages in subjective well-being and perceived youthfulness compared to their peers [5, 8, 9]. Empirical evidence from large-scale longitudinal and daily-diary studies confirms that a non-trivial proportion of long-term couples consistently report frequent conflict yet maintain stable marriages with satisfaction and commitment levels comparable to or exceeding those of low-conflict couples [2, 3]. This directly challenges the traditional notion that low conflict equals high stability, offering a novel insight into the mechanisms of stability in marital relationships.

While previous research has laid a multi-dimensional framework for understanding marital stability, several key gaps remain. In conflict-stability studies, Gottman and Levenson [10] categorized marital conflicts as destructive or constructive, emphasizing that conflict resolution styles, rather than frequency, predict marital dissolution. However, they did not address the co-evolution of periodic large conflicts and intimacy repair, leaving unanswered the question of why some high-conflict couples remain intact. Huston et al. [11], using a 13-year longitudinal dataset, outlined a honeymoon-decline-stability trajectory of marital quality, yet their analysis did not quantify the alternating dynamics of conflict and intimacy. Similarly, Karney and Bradbury [12] highlighted the role of endogenous repair behaviors in mitigating conflict damage but did not examine how repair intensity relates to conflict severity or the feedback loop of crises fostering appreciation. At the mathematical modeling level, previous approaches, including Rusbult's Investment Model [13], Gottman et al.'s nonlinear systems [14], and Barnes et al.'s marital interaction model for Ghana [15], rely on deterministic equations that fail to capture the randomness of conflict events and their varying intensities. While recent stochastic models, such as those proposed by Herrera de la Cruz and Rey [16] and Abreu-Afonso et al. [17], have advanced the field, they overlooked the intricate interplay between conflicts and repair dynamics, key elements of the dynamically balanced marital pattern.

Recent developments in numerical methods for evolution equations have further advanced stability analyses through high-order compact schemes and alternating-direction implicit (ADI) techniques. For example, high-order compact Crank–Nicolson ADI schemes on graded meshes have been applied to three-dimensional nonlinear partial integro-differential equations (PIDEs) with multiple weakly singular kernels [18]. These approaches, together with structure-preserving techniques such as positivity-preserving finite volume schemes on distorted meshes and superconvergence analyses for subdiffusion equations, collectively underscore the growing emphasis on efficient, unconditionally stable, and

physically consistent discretizations—principles that directly inform our design of a bounded state space $[0, 1]^2$ and the rigorous proof of ergodic convergence, thereby ensuring realistic long-term marital dynamics.

These gaps point to the need for further exploration in three areas: the dynamic mechanisms of alternating conflict and intimacy, the quantitative modeling of random events, and the functional transformation of conflicts—the empirically observed process whereby frequent conflict serves not to erode but to sustain emotional engagement and prevent intimacy stagnation [2]—within marital relationships. To address these gaps, the present work develops a bivariate stochastic pure-jump framework that explicitly incorporates the hierarchical structure of conflicts (frequent small conflicts and rare large conflicts) and spontaneous endogenous repair events. By modeling both the timing (via independent Poisson processes) and magnitude (via uniform-distributed jumps) of these events within a bounded state space $[0, 1]^2$, the model captures the alternating conflict–intimacy dynamics characteristic of stably balanced marriages. Rigorous theoretical analysis establishes solution existence, uniqueness and boundedness as well as the existence of a unique ergodic stationary distribution, and extensive numerical experiments and global sensitivity analysis reveal the dominant roles of intimacy recovery rate and positive repair frequency in sustaining long-term stability despite persistent conflict.

The remainder of the paper is structured as follows: Section 2 introduces a system of stochastic differential equations to model intimacy and conflict evolution, grounded in the concept of dual randomness (time and magnitude); Section 3 presents the core theoretical results, including the existence and uniqueness of solutions, state boundedness, stochastic stability of intimacy, and convergence to a unique stationary distribution; Section 4 provides detailed mathematical proofs to rigorously validate the theoretical soundness of the model; Section 5 presents numerical simulations, illustrating the dynamic interaction of intimacy and conflict; Section 6 performs sensitivity analysis to quantify the impact of key parameters on marital stability; and Section 7 discusses the theoretical and methodological contributions of this study, outlines the limitations of current mathematical models, and proposes future directions for integrating sociological and psychological empirical data into model development.

2. Mathematical modeling

This study focuses on an undertheorized dynamically balanced marital pattern in couple interactions: in long-term cohabitation, conflict and intimacy are not simply negatively correlated but alternate rhythmically. With high conflict frequency or intensity, relationships remain intact and sustain long-term stability. Indicators like individuals' subjective well-being and physical vitality do not decline significantly; these metrics even outperform those for traditional low-conflict/high-stability control groups. Accordingly, we model the phenomenon as a generalized dynamical problem to explore its stability mechanism.

2.1. Problem analysis

The dynamic characteristics of conflict and repair in couple interactions are central to describing relationship stability. To address the three research gaps identified in the Section 1 (dynamic mechanisms of alternating conflict and intimacy, quantitative modeling of random events, and functional transformation of conflicts), this study aims to fulfill three key modeling tasks: first, to clarify the dynamic mechanism underlying the alternation between conflict and intimacy; second, to quantify the

hierarchical characteristics and stochastic patterns of conflict/repair events; third, to verify the stability mechanism of dynamically balanced marriages through theoretical analysis and numerical simulations.

Relationship repair in this marital pattern is distinctly endogenous, initiating entirely from the couple without external interventions. This requires two core modeling considerations: repair effects must be state-dependent rather than fixed-magnitude to align with real relationship dynamics, and repair timing and form must be stochastic to reflect its unplanned nature. Additionally, the pattern's most striking feature, high conflict frequency alongside long-term stability, demands clear state boundaries: intimacy and conflict intensity must be bounded within reasonable ranges to avoid relationship breakdown or family function failure, with intimacy fluctuating around a relatively high long-term baseline to reflect observed physical and psychological advantages.

From this analysis, three core modelable characteristics emerge: First, conflict exhibits dual randomness, that is, two conflict types occur independently via stochastic processes with distinct intensities, and their impact magnitudes follow continuous distributions; second, an intimacy baseline regulates post-shock recovery, serving as the core stability mechanism; and third, endogenous repair behaviors act as compensatory positive events, random in timing and magnitude, that balance conflicts to maintain dynamic equilibrium.

2.2. Problem assumptions

Based on the problem analysis, we propose reasonable assumptions about this type of couple relationship.

1) Temporal continuity: The system state evolves over continuous time and follows the laws of stochastic differential equations.
2) Dual randomness of events: Both the occurrence of conflicts and positive events follow independent Poisson processes, and the impact magnitudes of events of the same type are random variables following a uniform distribution.
3) Baseline recoverability: There exists a baseline value for intimacy level; after a conflict or positive event, intimacy level reverts to the baseline under the effect of a recovery rate.
4) State boundedness: The impact magnitudes of conflict/repair events on the intimacy-conflict state are dynamically adjusted according to the current relationship level, ensuring no breakdown of the couple relationship.
5) Conflict attenuation: Conflict intensity decays naturally over time, and positive events can accelerate this decay; the impact magnitude of conflicts is a random variable within a specific interval.

2.3. Notation

To clearly characterize the evolution law of the intimacy–conflict dynamic system, standardize the notation for subsequent mathematical models, and ensure the rigor of equation construction and analysis, this section defines the state variables, event parameters (including stochastic processes), and global parameters involved in the model from three dimensions: "core system states", "event-related characteristics", and "global regulatory mechanisms", based on the previous modeling assumptions. This provides a clear notational reference for the construction of subsequent stochastic differential equations. Specific definitions are shown in Tables 1–3.

Table 1. Definition of system state variables.

Notation	Physical meaning	Value range
$I(t)$	Intimacy level at time t	$[0, 1]$ (0 = no connection, 1 = extreme intimacy)
$C(t)$	Conflict intensity at time t	$[0, 1]$ (0 = no conflict, 1 = extreme conflict)

Table 2. Event-related parameters and stochastic processes.

Event type	Poisson process	Intensity	Intimacy impact	Conflict impact
Small conflict	$N_{\mathrm{s}}(t)$	$\lambda_{\mathrm{s}} > 0$	$\Xi_{\mathrm{s}} \sim \mathrm{U}(a_{\mathrm{s}}, b_{\mathrm{s}})$	$\Gamma_{\mathrm{s}} \sim \mathrm{U}(c_{\mathrm{s}}, d_{\mathrm{s}})$
Large conflict	$N_{\mathrm{l}}(t)$	$\lambda_{\mathrm{l}} > 0$	$\Xi_{\mathrm{l}} \sim \mathrm{U}(a_{\mathrm{l}}, b_{\mathrm{l}})$	$\Gamma_{\mathrm{l}} \sim \mathrm{U}(c_{\mathrm{l}}, d_{\mathrm{l}})$
Positive event	$N_{\mathrm{p}}(t)$	$\lambda_{\mathrm{p}} > 0$	$\Xi_{\mathrm{p}} \sim \mathrm{U}(a_{\mathrm{p}}, b_{\mathrm{p}})$	$\Gamma_{\mathrm{p}} \sim \mathrm{U}(c_{\mathrm{p}}, d_{\mathrm{p}})$

[1] Subscripts: s = small conflict, l = large conflict, p = positive event;

[2] Impact direction: $\Xi_{\mathrm{s/l}}$ (negative), Ξ_{p} (positive); $\Gamma_{\mathrm{s/l}}$ (positive), Γ_{p} (negative);

[3] $\mathrm{U}(a, b)$: uniform distribution over interval (a, b), where a, b denote bounds of impact magnitude intervals;

[4] "Intensity" refers to Poisson intensity ($\lambda_k > 0$); Ξ/Γ denote random impact magnitudes of events.

2.4. Mathematical model

The intimacy–conflict dynamic model is described by the following system of stochastic differential equations with random amplitude jumps:

$$\begin{cases} dI(t) = r_I(I_{\mathrm{baseline}} - I(t))dt + \sum_{k=1}^{3} \Xi_k(t)\, dN_k(t), \\ dC(t) = -r_C C(t)dt + \sum_{k=1}^{3} \Gamma_k(t)\, dN_k(t), \end{cases} \tag{2.1}$$

with initial conditions

$$I(0) = I_{\mathrm{baseline}}, \quad C(0) = 0.$$

Here, $N_k(t)$ ($k = 1, 2, 3$) correspond to the independent Poisson processes $N_{\mathrm{s}}(t)$, $N_{\mathrm{l}}(t)$, and $N_{\mathrm{p}}(t)$, respectively, with intensities $\lambda_k > 0$. The intimacy impact processes $\{\Xi_k(t)\}$ are defined as $\Xi_1 = -\Xi_{\mathrm{s}}$, $\Xi_2 = -\Xi_{\mathrm{l}}$, and $\Xi_3 = +\Xi_{\mathrm{p}}$. The conflict impact processes $\{\Gamma_k(t)\}$ are defined as $\Gamma_1 = +\Gamma_{\mathrm{s}}$, $\Gamma_2 = +\Gamma_{\mathrm{l}}$, and $\Gamma_3 = -\Gamma_{\mathrm{p}}$. Both $\{\Xi_k\}$ and $\{\Gamma_k\}$ are independent of $\{N_k\}$ and adapted to the filtration.

In model (2.1), the drift term $r_I(I_{\mathrm{baseline}} - I(t))dt$ in the intimacy equation drives intimacy to fluctuate around the baseline, while the jump term $\sum \Xi_k dN_k$ captures random event impacts (conflicts reduce intimacy, whereas positive events increase it, with magnitudes fluctuating within reasonable ranges). Similarly, the drift term $-r_C C(t)dt$ in the conflict equation reflects natural conflict decay, and the jump term $\sum \Gamma_k dN_k$ captures random event effects (conflicts intensify conflict intensity, whereas positive events alleviate it, with random magnitudes).

Table 3. Definition of system global parameters.

Notation	Physical meaning	Value range/Attribute
I_{baseline}	Intimacy baseline	$(0, 1)$ (constant)
r_I	Intimacy recovery rate	> 0 (constant)
r_C	Conflict intensity decay rate	> 0 (constant)

The core logic combines dual randomness (Poisson event timings, uniform impact magnitudes) with recovery/decay mechanisms, enabling intimacy to fluctuate around the baseline and conflicts to maintain dynamic balance, consistent with real relationship interactions. Thus, although the continuous drift of $I(t)$ is mean-reverting only to its own baseline, and no explicit diffusion coupling term is present, the two processes remain strongly interdependent through shared jump times triggered by the same Poisson clocks $N_k(t)$ and, most crucially, the state-dependent truncation of jump magnitudes that explicitly depends on the current conflict intensity $C(t)$.

We adopt uniform jump magnitudes and independent Poisson clocks for three key reasons that directly address potential distributional ambiguity.

1) Robustness and identifiability: with currently scarce high-resolution daily-diary data on exact marital event magnitudes, two-parameter uniform distributions minimize overfitting risk and ensure parameter identifiability during future calibration.

2) Neutrality: unlike exponential (heavily right-skewed) or Gaussian (unbounded) alternatives, uniform distribution imposes no a priori bias on impact skewness, which is ideal when exploring an understudied pattern for the first time.

3) Empirical consistency: inter-arrival times of marital conflicts and positive events in daily-diary studies (e.g., Birditt et al. [3]; Rafaeli et al. [9]) pass standard tests for exponential distribution, strongly supporting independent Poisson clocks. Alternative bounded distributions (Beta, truncated normal) or state-dependent processes (Hawkes, Markov-modulated Poisson) are natural extensions and will be pursued once larger calibrated datasets become available, but they are deliberately deferred here to keep the model parsimonious and focused on the core stability mechanisms.

2.5. Equivalence of compensated and non-compensated measure representations

The main model (2.1) is initially formulated using *non-compensated* Poisson processes $N_k(t)$, which directly characterize the random occurrence of real-world events (small conflicts, large conflicts, positive events). However, for rigorous mathematical analysis (e.g., proving existence/uniqueness of solutions), we convert the model to a *compensated* Poisson measure representation, a pure-jump stochastic differential equation (SDE), following Lemma 4.2. This subsection clarifies the equivalence of the two formulations and the origin of the additional drift terms β_I and β_C.

2.5.1. Decomposition of non-compensated Poisson processes

By definition, a non-compensated Poisson process $N_k(t)$ with intensity λ_k can be decomposed into

$$dN_k(t) = d\widetilde{N}_k(t) + \lambda_k dt,$$

where $\widetilde{N}_k(t) = N_k(t) - \lambda_k t$ is the *compensated Poisson process* (martingale). Substituting this into the jump terms of model (2.1) yields

$$\sum_{k=1}^{3} \Xi_k dN_k(t) = \sum_{k=1}^{3} \Xi_k d\widetilde{N}_k(t) + \sum_{k=1}^{3} \lambda_k \Xi_k dt,$$

$$\sum_{k=1}^{3} \Gamma_k dN_k(t) = \sum_{k=1}^{3} \Gamma_k d\widetilde{N}_k(t) + \sum_{k=1}^{3} \lambda_k \Gamma_k dt.$$

Taking expectations of the deterministic components (because Ξ_k, Γ_k are independent of $N_k(t)$),

$$\mathbb{E}\left[\sum_{k=1}^{3} \lambda_k \Xi_k\right] = \sum_{k=1}^{3} \lambda_k \mathbb{E}[\Xi_k] = \beta_I, \quad \mathbb{E}\left[\sum_{k=1}^{3} \lambda_k \Gamma_k\right] = \sum_{k=1}^{3} \lambda_k \mathbb{E}[\Gamma_k] = \beta_C.$$

2.5.2. Equivalent compensated SDE formulation

Substituting the decomposition into model (2.1), we obtain the compensated measure representation

$$dX(t) = \alpha(X(t))dt + \int_{\mathbb{R}^2} \gamma(z)\widetilde{N}(dt, dz),$$

where $X(t) = (I(t), C(t))^\top$, the drift vector $\alpha(X)$ is

$$\alpha(X) = \begin{pmatrix} r_I(I_{\text{baseline}} - I) + \beta_I \\ -r_C C + \beta_C \end{pmatrix},$$

and $\gamma(z) = (\Xi_k, \Gamma_k)^\top$ denotes the jump size vector.

2.5.3. Interpretation of the additional drift terms

The terms β_I and β_C are not "extra" but arise from the mathematical separation of the *mean drift* (deterministic) and *martingale jump* (stochastic) components of Poisson processes. For the dynamically balanced marital pattern, $\beta_I \approx 0$ and $\beta_C \approx 0$ (the positive/negative impacts of events offset over time) align with the empirical observation of "long-term equilibrium" in such relationships.

This equivalence ensures the original model's interpretability (non-compensated form) and the analysis's rigor (compensated form), resolving potential confusion about the drift term composition.

3. Main results

The model (2.1) is a *pure-jump* SDE driven solely by three compensated Poisson random measures with no diffusion component. All subsequent theoretical results rely exclusively on techniques for discontinuous semimartingales.

We now present the principal theoretical contributions of this paper concerning the intimacy–conflict model (2.1). These theoretical results are not merely formal exercises, they directly underpin the model's ability to explain the dynamically balanced marital pattern, as detailed below.

Theorem 3.1 (Existence and uniqueness of solutions)**.** *For the initial condition* $(I(0), C(0)) = (I_{\text{baseline}}, 0)$ *with* $I_{\text{baseline}} \in (0, 1)$*, the stochastic differential equation* (2.1) *admits a unique càdlàg adapted solution* $(I(t), C(t))_{t\geq 0}$*. Moreover, for every* $T < \infty$*,*

$$\mathbb{E}\left[\sup_{0\leq t\leq T} \left(|I(t)|^2 + |C(t)|^2\right)\right] < \infty.$$

Theorem 3.2 (State boundedness)**.** *Under the state-dependent truncation mechanism introduced in Section 2.2, the trajectories satisfy almost surely*

$$0 \leq I(t) \leq 1, \qquad 0 \leq C(t) \leq 1 \quad \textit{for all } t \geq 0.$$

Thus, the state $(I(t), C(t))$ *remains confined to the unit square* $[0, 1]^2$ *with probability one.*

Theorem 3.3 (Bounded long-term fluctuations of intimacy)**.** *For every $\varepsilon > 0$,*

$$\limsup_{t\to\infty} \mathbb{P}(|I(t) - I_{\text{baseline}}| > \varepsilon) \le \frac{2K}{c\varepsilon^2},$$

where $c = 2r_I > 0$ and $K = \frac{3}{2}(\lambda_s + \lambda_l + \lambda_p)$. This quantifies the concentration of intimacy around its baseline in the long run.

Theorem 3.4 (Unique stationary distribution)**.** *The process $(I(t), C(t))_{t\ge0}$ is positive Harris recurrent and possesses a unique invariant probability measure π on $[0,1]^2$. For any initial condition in $[0,1]^2$, the distribution of $(I(t), C(t))$ converges weakly to π as $t \to \infty$.*

We stress that Theorems 3.2–3.4 establish purely mathematical properties: the process is positive Harris recurrent and admits a unique ergodic invariant measure π on $[0,1]^2$, implying that time averages converge almost surely to π-expectations with persistently high $\mathbb{E}_\pi[I]$ and low $\mathbb{E}_\pi[C]$. This probabilistic long-run behaviour is fully consistent with the empirical observation that a nontrivial proportion of couples exhibit frequent conflict yet sustain high intimacy and do not dissolve over decades [2, 3, 5]. However, the existence of a unique stationary distribution is neither necessary nor sufficient to rigorously prove that any specific individual marriage will never end in divorce; it merely provides the quantitative statistical signature that matches the population-level phenomenon of dynamically balanced marriages. The proofs of Theorems 3.1–3.4 are deferred to Section 4. Monte Carlo estimation under calibrated parameters yields $\mathbb{E}_\pi[I] \approx 0.766$ and $\mathbb{E}_\pi[C] \approx 0.117$ (Figure 1), in excellent quantitative agreement with longitudinal studies of high-conflict yet enduring marriages.

4. Proofs of the main results

In this section, we provide detailed proofs of the four main theorems stated in Section 3. All auxiliary lemmas are numbered locally within this section. The analytical results presented below deliberately employ established techniques from stochastic analysis. Their originality lies not in the invention of new general theorems, but in the careful construction and rigorous verification of a tailored modelling framework that, for the first time, quantitatively reproduces the paradoxical yet robust empirical phenomenon of dynamically balanced marriages. The following proofs use ergodic theory to rigorously validate the model's core behavioral predictions, ensuring that the observed long-term stability and recovery dynamics are mathematically grounded rather than purely empirical.

4.1. Proof of Theorem 3.1 (Existence and uniqueness)

Lemma 4.1 (Existence and uniqueness of solutions to pure-jump Poisson-driven SDE, directly cited from Theorem 1.19 in [19])**.** *Consider the pure-jump Poisson-driven SDE in $\mathbb{R}^n$:*

$$dX(t) = \alpha(t, X(t))\,dt + \sigma(t, X(t))\,dB(t) + \int_{\mathbb{R}^n} \gamma(t, X(t^-), z)\,\widetilde{N}(dt, dz), \quad X(0) = x_0 \in \mathbb{R}^n,$$

where α, σ, and γ are measurable adapted functions; $B(t)$ is an m-dimensional Brownian motion; $\widetilde{N}(dt, dz)$ is a compensated Poisson random measure with Lévy measure ν satisfying $\int_{\mathbb{R}^n}(1 \wedge |z|^2)\nu(dz) < \infty$; and $X(t^-)$ denotes the left-hand limit of $X(t)$ at time t.

Suppose the following linear growth condition and Lipschitz continuity condition are satisfied:

1) Linear growth condition: There exists a constant $C_1 < \infty$ such that

$$\|\sigma(t,x)\|^2 + |\alpha(t,x)|^2 + \int_{\mathbb{R}^n} |\gamma(t,x,z)|^2 \nu(dz) \le C_1(1+|x|^2).$$

2) Lipschitz continuity condition: There exists a constant $C_2 < \infty$ such that

$$\|\sigma(t,x)-\sigma(t,y)\|^2 + |\alpha(t,x)-\alpha(t,y)|^2 + \int_{\mathbb{R}^n} |\gamma(t,x,z)-\gamma(t,y,z)|^2 \nu(dz) \le C_2|x-y|^2.$$

Then the equation has a unique right-continuous with left limits (càdlàg) adapted solution $X(t)$, and for all $t \ge 0$, $\mathbb{E}[|X(t)|^2] < \infty$ holds.

Lemma 4.2 (Representation of compensated measure for Poisson jumps)**.** *Let $\{N_k(t)\}_{k=1}^m$ be independent Poisson processes with intensities $\lambda_k > 0$. The jump size (mark) of the kth type of event is a vector $Z_k^{(i)} \in \mathbb{R}^d$, and $\{Z_k^{(i)}\}_{i\ge1}$ are independent and identically distributed with probability measure μ_k, satisfying $\int_{\mathbb{R}^d}(1 \wedge \|z\|^2)\,\mu_k(dz) < \infty$, and there exists a constant M_k such that $\|Z_k^{(i)}\| \le M_k < \infty$ a.s.*

Define the compound jump process:

$$J(t) = \sum_{k=1}^{m} \sum_{i=1}^{N_k(t)} Z_k^{(i)}.$$

Let the overall Lévy measure be $\nu(dz) = \sum_{k=1}^m \lambda_k \mu_k(dz)$, and the Poisson random measure be

$$N(dt,dz) = \sum_{k=1}^{m} \sum_{i\ge1} \delta_{(T_k^{(i)}, Z_k^{(i)})}(dt,dz),$$

with mean measure $\mathbb{E}[N(dt,dz)] = \nu(dz)dt$. Then

$$J(t) = \int_0^t \int_{\mathbb{R}^d} z\,\widetilde{N}(ds,dz) + \int_0^t \Big(\int_{\mathbb{R}^d} z\,\nu(dz) \Big) ds,$$

where $\widetilde{N}(dt,dz) = N(dt,dz) - \nu(dz)dt$ is the compensated Poisson measure.

Proof. By definition, the Poisson random measure can be expressed as

$$N(dt,dz) = \sum_{k,i} \delta_{(T_k^{(i)}, Z_k^{(i)})}(dt,dz),$$

with mean measure $\nu(dz)dt$. Under the integrability assumption of jump sizes, $\int_{\mathbb{R}^d}(1 \wedge \|z\|^2)\nu(dz) < \infty$ holds, so the compensated measure

$$\widetilde{N}(dt,dz) = N(dt,dz) - \nu(dz)dt$$

is well-defined.

The compound jump process can be rewritten in the integral form of the random measure:

$$J(t) = \int_0^t \int_{\mathbb{R}^d} z\,N(ds,dz).$$

Substituting the decomposition of the compensated measure $N = \widetilde{N} + \nu ds$, we obtain

$$J(t) = \int_0^t \int_{\mathbb{R}^d} z\, \widetilde{N}(ds, dz) + \int_0^t \int_{\mathbb{R}^d} z\, \nu(dz)\, ds.$$

Because the first moment $\mathbb{E}[Z_k^{(i)}]$ of each type of jump size exists, the second term in the above equation is finite. This completes the proof. □

Proof of Theorem 3.1. Denote the state vector $X(t) = (I(t), C(t))^\top \in \mathbb{R}^2$. Using Lemma 4.2, the compound Poisson jump terms in the model can be expressed in the form of a compensated measure integral:

$$dX(t) = \alpha(X(t))\, dt + \int_{\mathbb{R}^2} \gamma(z)\, \widetilde{N}(dt, dz),$$

where

$$\alpha(X) = \begin{pmatrix} r_I(I_{\text{baseline}} - I) + \beta_I \\ -r_C C + \beta_C \end{pmatrix}, \quad \gamma(z) = (\Xi_k, \Gamma_k)^\top,$$

and the constant compensation terms are

$$\beta_I = \sum_k \lambda_k \mathbb{E}[\Xi_k], \quad \beta_C = \sum_k \lambda_k \mathbb{E}[\Gamma_k].$$

The jump size components satisfy $|\Xi_k|, |\Gamma_k| \le 1$ a.s. We verify the conditions of Lemma 4.1 step by step below.

First, verify the linear growth condition. Using the inequality $|a + b|^2 \le 2(|a|^2 + |b|^2)$, we have

$$|\alpha(X)|^2 \le C_{11} + C_{12}|X|^2,$$

where C_{11} and C_{12} are positive constants. For the jump term, because $\|\gamma(z)\|^2 = \Xi_k^2 + \Gamma_k^2 \le 1 + 1 = 2$, combined with the finiteness of the Lévy measure,

$$\int_{\mathbb{R}^2} \|\gamma(z)\|^2 \nu(dz) \le 2 \int_{\mathbb{R}^2} \nu(dz) \le C_{13},$$

where C_{13} is a constant. Thus, there exists $C_1 < \infty$ such that

$$|\alpha(X)|^2 + \int_{\mathbb{R}^2} \|\gamma(z)\|^2 \nu(dz) \le C_1(1 + |X|^2).$$

Next, verify the Lipschitz continuity condition. Direct calculation gives

$$|\alpha(X_1) - \alpha(X_2)|^2 \le (r_I^2 + r_C^2)|X_1 - X_2|^2.$$

Because the jump kernel $\gamma(z)$ is independent of the state X, the integral term is zero. Thus, there exists a constant $C_2 = r_I^2 + r_C^2$ such that

$$|\alpha(X_1) - \alpha(X_2)|^2 + \int_{\mathbb{R}^2} \|\gamma(z, X_1) - \gamma(z, X_2)\|^2 \nu(dz) \le C_2 |X_1 - X_2|^2.$$

Therefore, the model satisfies all conditions of Lemma 4.1, so there exists a unique càdlàg adapted solution with finite second moments. □

4.2. Proof of Theorem 3.2 (State boundedness)

In Section 2, Subsection 2.2, we have assumed that "the impact magnitudes of conflict/repair events on the intimacy–conflict state are dynamically adjusted according to the current relationship level". This is the core premise for ensuring the boundedness of solutions to the main model (2.1), and it also maps the adaptive adjustment ability in couple interactions.

Let the initial impact magnitudes of events on intimacy level and conflict intensity be $\Xi_{\mathrm{s}}^0, \Xi_{\mathrm{l}}^0, \Xi_{\mathrm{p}}^0 \in (0,1)$ and $\Gamma_{\mathrm{s}}^0, \Gamma_{\mathrm{l}}^0, \Gamma_{\mathrm{p}}^0 \in (0,1)$, respectively. Denote the instantaneous state immediately before an event occurs as

$$I^- \equiv I(t^-), \quad C^- \equiv C(t^-),$$

where t^- represents the instantaneous moment before the event occurs. The actual impact magnitudes acting on the system are truncated in a state-dependent manner:

$$\begin{aligned}
&\Xi_{\mathrm{s}} = \min(\Xi_{\mathrm{s}}^0, I^-), && \Xi_{\mathrm{l}} = \min(\Xi_{\mathrm{l}}^0, I^-), && \Xi_{\mathrm{p}} = \min(\Xi_{\mathrm{p}}^0, 1 - I^-),\\
&\Gamma_{\mathrm{s}} = \min(\Gamma_{\mathrm{s}}^0, 1 - C^-), && \Gamma_{\mathrm{l}} = \min(\Gamma_{\mathrm{l}}^0, 1 - C^-), && \Gamma_{\mathrm{p}} = \min(\Gamma_{\mathrm{p}}^0, C^-),
\end{aligned}$$

which ensures that the state remains within $[0,1]^2$ (a.s.) after the event occurs, that is,

$$0 < |\Xi_k(t)| < 1, \quad 0 < |\Gamma_k(t)| < 1.$$

Notably, the system exhibits no sticky or absorbing behavior at boundaries. Whenever $I = 0$ or $I = 1$ is reached via a jump, the mean-reverting drift acts instantaneously to repel the state inward, for example, $I = 0$ triggers a positive drift toward I_{baseline}, whereas $I = 1$ induces a negative drift. For $C = 0$ and $C = 1$, the conflict decay drift or event jumps similarly drive rapid recovery to interior states. This combination of hard truncation and immediate drift ensures dynamic activity within $[0,1]^2$, consistent with empirical observations of spontaneous relationship recovery.

This mechanism not only provides a guarantee for mathematical boundedness but also reflects the adaptive adjustment based on the current relationship level in couple interactions. It balances conflict impacts and relationship stability, characterizing the stability and adaptability of the dynamic evolution of relationships.

Proof of Theorem 3.2. The proof proceeds by mathematical induction on the event times, combined with the continuous evolution between events.

Initial condition. By construction, $I(0) = I_{\mathrm{baseline}} \in (0,1)$ and $C(0) = 0$, so $0 \le I(0) \le 1$ and $0 \le C(0) \le 1$.

At event times. Let $\{t_k\}_{k\ge1}$ be the successive event times and assume $0 \le I(t_k^-) \le 1$, $0 \le C(t_k^-) \le 1$. For the intimacy component after the k-th event,

$$\begin{aligned}
I(t_k^+) &= I(t_k^-) - \Xi_{\mathrm{s/l}} + \Xi_{\mathrm{p}} \ge I(t_k^-) - I(t_k^-) + 0 = 0,\\
I(t_k^+) &= I(t_k^-) - \Xi_{\mathrm{s/l}} + \Xi_{\mathrm{p}} \le I(t_k^-) + (1 - I(t_k^-)) = 1,
\end{aligned}$$

where the inequalities follow directly from the state-dependent truncation rules above. An analogous argument shows $0 \le C(t_k^+) \le 1$.

Between events. On any interval (t_k, t_{k+1}) with no events, the process is governed by the deterministic ordinary differential equation (ODE)

$$\frac{dI(t)}{dt} = r_I(I_{\mathrm{baseline}} - I(t)), \qquad \frac{dC(t)}{dt} = -r_C C(t).$$

The solution for $I(t)$ is monotone and remains in $[\min(I(t_k^+), I_{\text{baseline}}), \max(I(t_k^+), I_{\text{baseline}})] \subset (0, 1)$. The solution for $C(t)$ is $C(t) = C(t_k^+)e^{-r_C(t-t_k)} \in [0, C(t_k^+)] \subset [0, 1]$.

By induction, $0 \le I(t) \le 1$ and $0 \le C(t) \le 1$ hold almost surely for all $t \ge 0$. □

4.3. Proof of Theorem 3.3 (Bounded long-term fluctuations of intimacy)

Lemma 4.3 (Itô's formula for processes with jumps, directly cited from Theorem 1.14 in [19])**.** *Suppose $X(t)$ is an Itô–Lévy process of the form*

$$dX(t) = \alpha(t, \omega)dt + \sigma(t, \omega)dB(t) + \int_{\mathbb{R}} \gamma(t, z, \omega)\tilde{N}(dt, dz),$$

where $\tilde{N}(dt, dz) = N(dt, dz) - \nu(dz)dt$ denotes the compensated Poisson random measure. If $f \in C^2(\mathbb{R}^2)$, define $Y(t) = f(t, X(t))$; then $Y(t)$ is also an Itô–Lévy process, satisfying

$$\begin{aligned} dY(t) = &\frac{\partial f}{\partial t}(t, X(t))dt + \frac{\partial f}{\partial x}(t, X(t))dX(t) \\ &+ \frac{1}{2}\sigma^2(t, \omega)\frac{\partial^2 f}{\partial x^2}(t, X(t))dt \\ &+ \int_{\mathbb{R}} \left[f(t, X(t^-) + \gamma(t, z)) - f(t, X(t^-))\right] N(dt, dz). \end{aligned} \tag{4.1}$$

Lemma 4.4 (Expectation properties of Poisson random measures, directly cited from Theorem 1.5 in [19])**.** *Let $N(t, U)$ be the Poisson random measure of a Lévy process, which counts the number of jumps with magnitudes in the Borel set $U \subset B_0$ (where B_0 denotes a Borel set whose closure does not contain 0). It satisfies the following properties: 1) The Lévy measure is defined as $\nu(U) = \mathbb{E}[N(1, U)]$, representing the expected number of jumps with magnitudes in U per unit time; 2) For disjoint sets $U_k \in B_0$, let $N_k(t) = N(t, U_k)$ (independent Poisson processes), with intensity $\lambda_k = \nu(U_k)$; 3) The instantaneous expectation of the Poisson process satisfies*

$$\mathbb{E}[dN_k(t)] = \lambda_k dt,$$

that is, the instantaneous expectation equals the product of intensity and time increment.

Lemma 4.5 (Application of Markov inequality to bounded fluctuations of intimacy level)**.** *Let the deviation Lyapunov function for the intimacy level $I(t)$ be*

$$V(I) = \frac{1}{2}(I - I_{baseline})^2 \ge 0, \quad \forall I \in [0, 1].$$

Suppose there exists a constant $\epsilon > 0$ such that the event equivalence relation

$$|I(t) - I_{baseline}| > \epsilon \iff V(I(t)) > \frac{\epsilon^2}{2}$$

holds. If

$$\limsup_{t\to\infty} \mathbb{E}[V(I(t))] = \frac{K}{c} \quad (K > 0, c > 0),$$

then the probability that the intimacy level deviates from the baseline by more than ϵ satisfies

$$\limsup_{t\to\infty} \mathbb{P}(|I(t) - I_{baseline}| > \epsilon) \le \frac{2K}{c\,\epsilon^2}.$$

Proof. By definition, $V(I(t))$ is a nonnegative random variable. Applying the Markov inequality, for any threshold $a > 0$, we have

$$\mathbb{P}(V(I(t)) > a) \leq \frac{\mathbb{E}[V(I(t))]}{a}.$$

Set $a = \frac{\epsilon^2}{2}$ and use the event equivalence relation

$$\mathbb{P}(|I(t) - I_{\text{baseline}}| > \epsilon) = \mathbb{P}\Big(V(I(t)) > \frac{\epsilon^2}{2}\Big),$$

which gives

$$\mathbb{P}(|I(t) - I_{\text{baseline}}| > \epsilon) \leq \frac{2\,\mathbb{E}[V(I(t))]}{\epsilon^2}.$$

Taking the limsup ($\limsup_{t\to\infty}$) on both sides,

$$\limsup_{t\to\infty} \mathbb{P}(|I(t) - I_{\text{baseline}}| > \epsilon) \leq \frac{2}{\epsilon^2} \limsup_{t\to\infty} \mathbb{E}[V(I(t))].$$

Substituting the assumption $\limsup_{t\to\infty} \mathbb{E}[V(I(t))] = \frac{K}{c}$ yields the final result

$$\limsup_{t\to\infty} \mathbb{P}(|I(t) - I_{\text{baseline}}| > \epsilon) \leq \frac{2K}{c\,\epsilon^2}.$$

□

Proof of Theorem 3.3. Construct the Lyapunov function

$$V(I) = \frac{1}{2}(I - I_{\text{baseline}})^2,$$

which is nonnegative and characterizes the degree of deviation of the intimacy level from the baseline.

From the main model (2.1), the dynamics of $I(t)$ are given by

$$dI(t) = r_I(I_{\text{baseline}} - I)\,dt + \sum_{k=1}^{3} \Xi_k\,dN_k(t).$$

Apply Itô's formula for jump processes (Lemma 4.3) to $V(I(t))$:

$$dV(I(t)) = \mathcal{L}V(I(t))\,dt + \sum_{k=1}^{3} [V(I(t) + \Xi_k) - V(I(t))]dN_k(t),$$

where the generator $\mathcal{L}V$ is contributed solely by the drift term, calculated as

$$\mathcal{L}V(I) = \frac{\partial V}{\partial I} \cdot r_I(I_{\text{baseline}} - I) = -2r_I V(I).$$

Take the expectation of both sides and use the expectation property of Poisson processes (Lemma 4.4, i.e., $\mathbb{E}[dN_k(t)] = \lambda_k dt$):

$$\frac{d}{dt}\mathbb{E}[V(I(t))] = \mathbb{E}[\mathcal{L}V(I(t))] + \sum_{k=1}^{3} \lambda_k\,\mathbb{E}[V(I(t) + \Xi_k) - V(I(t))].$$

Step 1: Calculate the expectation of the drift term

$$\mathbb{E}[\mathcal{L}V(I(t))] = -2r_I\,\mathbb{E}[V(I(t))].$$

Step 2: Expand and estimate the expectation of the jump term Expand $V(I + \Xi_k) - V(I)$:

$$V(I + \Xi_k) - V(I) = (I - I_{\text{baseline}})\Xi_k + \frac{1}{2}\Xi_k^2.$$

Using the state boundedness $0 \le I(t) \le 1$ and magnitude constraint $0 < |\Xi_k| < 1$, we obtain

$$\left|(I - I_{\text{baseline}})\Xi_k + \tfrac{1}{2}\Xi_k^2\right| \le \frac{3}{2}.$$

Thus, the upper bound of the expectation of the jump term is

$$\sum_{k=1}^{3} \lambda_k\,\mathbb{E}[V(I + \Xi_k) - V(I)] \le \frac{3}{2}\sum_{k=1}^{3}\lambda_k = K.$$

Step 3: To establish and solve the differential inequality, combine the results of the drift and jump terms to obtain

$$\frac{d}{dt}\mathbb{E}[V(I(t))] \le -2r_I\,\mathbb{E}[V(I(t))] + K.$$

Let $c = 2r_I > 0$; the above inequality reduces to a first-order linear nonhomogeneous differential inequality,

$$\frac{d}{dt}\mathbb{E}[V(I(t))] \le -c\,\mathbb{E}[V(I(t))] + K.$$

Solving this inequality with the initial condition $V(0) = 0$,

$$\mathbb{E}[V(I(t))] \le \frac{K}{c}(1 - e^{-ct}),$$

which implies

$$\limsup_{t\to\infty} \mathbb{E}[V(I(t))] \le \frac{K}{c}.$$

Step 4: Derive the probability upper bound using the Markov inequality:

$$|I(t) - I_{\text{baseline}}| > \epsilon \iff V(I(t)) > \frac{\epsilon^2}{2}.$$

Applying the Markov inequality (Lemma 4.5) yields

$$\mathbb{P}(|I(t) - I_{\text{baseline}}| > \epsilon) \le \frac{2\,\mathbb{E}[V(I(t))]}{\epsilon^2}.$$

Taking the limsup as $t \to \infty$,

$$\limsup_{t\to\infty} \mathbb{P}(|I(t) - I_{\text{baseline}}| > \epsilon) \le \frac{2K}{c\epsilon^2}.$$

Conclusion: $I(t)$ is almost surely bounded and fluctuates around I_{baseline}. □

4.4. Proof of Theorem 3.4 (Unique stationary distribution)

Lemma 4.6 (Absorbability and unboundedness of solutions to drift conditions, directly cited from Theorem 15.2.2 in [20])**.** *Let the couple interaction process $(I(t), C(t))$ be ψ-irreducible, and suppose the function $V(I, C) : [0, 1]^2 \to [1, \infty]$ satisfies the drift condition*

$$\Delta V(I, C) \leq -\beta V(I, C) + b\mathbb{I}_C(I, C), \quad \forall (I, C) \in [0, 1]^2,$$

where $\Delta V(I, C) = PV(I, C) - V(I, C)$ (with $PV(I, C) = \mathbb{E}_{(I,C)}[V(I(1), C(1))]$ denoting the transition operator), $C \in \mathcal{B}([0, 1]^2)$ is a ν-small set, and $\beta > 0$, $b < \infty$ are constants. Then,

1) *The set $S_V = \{(I, C) : V(I, C) < \infty\}$ is either empty, or it is absorbing and full. Here, "absorbing" means that if $(I_0, C_0) \in S_V$, then $\mathbb{P}((I_0, C_0), S_V) = 1$; "full" means that $\pi(S_V) = 1$ (where π is the stationary distribution).*

2) *$V(I, C)$ is unbounded outside C: for any $M < \infty$, the set $\{(I, C) : V(I, C) \leq M\}$ remains a ν-small set.*

Lemma 4.7 (Drift equation for geometric kernels, directly cited from Theorem 15.2.3 in [20])**.** *Let $C \in \mathcal{B}([0, 1]^2)$ be a ν-small set, and let $r > 1$. Define the geometric kernel $G_C^{(r)}$ as*

$$G_C^{(r)}((I, C), \mathcal{U}) = \mathbb{E}_{(I,C)}\left[\sum_{k=0}^{\sigma_C} \mathbb{I}_{\mathcal{U}}(I(k), C(k))r^k\right],$$

where $\sigma_C = \inf\{k \geq 0 : (I(k), C(k)) \notin C\}$ (the first exit time from C) and $\mathcal{U} \subset [0, 1]^2$ is a measurable subset. Then,

$$PG_C^{(r)} = r^{-1}G_C^{(r)} - r^{-1}I + r^{-1}\mathbb{I}_C U_C^{(r)},$$

where I is the identity operator, and $U_C^{(r)}((I, C), \mathcal{U}) = \mathbb{E}_{(I,C)}\left[\sum_{k=1}^{\tau_C} \mathbb{I}_{\mathcal{U}}(I(k), C(k))r^k\right]$ (with $\tau_C = \inf\{k \geq 1 : (I(k), C(k)) \in C\}$ denoting the first return time).

Furthermore, let $\beta = 1 - r^{-1}$; then the drift operator satisfies:

$$\Delta G_C^{(r)} \leq -\beta G_C^{(r)} + r^{-1}\mathbb{I}_C U_C^{(r)}.$$

That is, $G_C^{(r)}$ is a solution to the drift condition.

Lemma 4.8. *[Geometric ergodicity theorem, directly cited from Theorem 15.0.1 in [20]] Let the couple interaction process $(I(t), C(t))$ be ψ-irreducible and aperiodic. Then the following three conditions are equivalent:*

1) *The process is positive recurrent with an invariant probability measure π; there exists a ν-small set $C \in \mathcal{B}^+([0, 1]^2)$, constants $\rho_C < 1$, $M_C < \infty$, and $P^\infty(C) > 0$ such that for all $(I, C) \in C$,*

$$|P^n((I, C), C) - P^\infty(C)| \leq M_C\rho_C^n.$$

2) *There exists a ν-small set $C \in \mathcal{B}([0, 1]^2)$ and a constant $\kappa > 1$ such that*

$$\sup_{(I,C)\in C} \mathbb{E}_{(I,C)}[\kappa^{\tau_C}] < \infty.$$

3) There exists a ν-small set $C \in \mathcal{B}([0,1]^2)$, constants $\beta > 0$, $b < \infty$, and a function $V \geq 1$ (finite at some $(I_0, C_0) \in [0,1]^2$) such that

$$\Delta V(I,C) \leq -\beta V(I,C) + b\mathbb{I}_C(I,C), \quad \forall (I,C) \in [0,1]^2. \tag{4.2}$$

If any of these conditions holds, it implies that $S_V = \{(I,C) : V(I,C) < \infty\}$ is absorbing and full, and there exist constants $r > 1$, $R < \infty$ such that for all $(I,C) \in S_V$,

$$\sum_{n=1}^{\infty} r^n \|P^n((I,C),\cdot) - \pi\|_V \leq RV(I,C),$$

where $\|\mu - \pi\|_V = \sup_{f:|f|\leq V} |\mu(f) - \pi(f)|$ denotes the V-norm.

Definition 4.1 (Weak convergence, Chapter 1 in [21])**.** *Let $\{\mathcal{D}_t\}_{t\geq 0}$ be the family of probability distributions for $(I(t), C(t))$. If there exists a probability distribution π such that for any bounded continuous function $f : [0,1]^2 \to \mathbb{R}$,*

$$\lim_{t\to\infty} \int_{[0,1]^2} f(x,y)\mathcal{D}_t(dx,dy) = \int_{[0,1]^2} f(x,y)\pi(dx,dy),$$

then $\mathcal{D}_t$ is said to converge weakly to π, denoted as $\mathcal{D}_t \xrightarrow[t\to\infty]{weakly} \pi$.

Definition 4.2 (Stationary distribution, Theorem 1.3.1 in [20])**.** *A probability distribution π is called a stationary distribution of the stochastic process $(I(t), C(t))$ if for any $t \geq 0$ and measurable set $A \subset [0,1]^2$,*

$$\int_{[0,1]^2} \mathbb{P}((I(t), C(t)) \in A \mid (I(0), C(0)) = (x,y))\pi(dx,dy) = \pi(A).$$

Proof of Theorem 3.4. The proof is completed in six steps by verifying all prerequisites of Lemma 4.8, combined with Lemmas 4.6 and 4.7:

Step 1: The system is a strong Markov process. From the structure of model (2.1), the drift term $b_I(I) = r_I(I_{\text{baseline}} - I)$ depends only on the current $I(t)$, and the drift term for conflict intensity $b_C(C) = -r_C C$ depends only on the current $C(t)$; neither depends on historical states. The jump terms are driven by independent Poisson processes $N_{\text{s}}(t)$, $N_{\text{l}}(t)$, and $N_{\text{p}}(t)$, which also satisfy the Markov property.

By the definition of strong Markovity, for any stopping time τ and $t \geq 0$,

$$\mathbb{P}((I(\tau+t), C(\tau+t)) \in A \mid \mathcal{F}_\tau) = \mathbb{P}((I(\tau+t), C(\tau+t)) \in A \mid (I(\tau), C(\tau))),$$

where $\mathcal{F}_\tau$ is the filtration up to time τ. Thus, the system satisfies the strong Markov property, meeting the process type requirement of Lemma 4.8. Moreover, because the state space $[0,1]^2$ is compact, the drift coefficients $b_I(I)$ and $b_C(C)$ are Lipschitz continuous (hence, uniformly continuous), and the Poisson intensities $\lambda_{\text{s}}, \lambda_{\text{l}}, \lambda_{\text{p}}$ are positive constants (state-independent), the transition semigroup is automatically Feller continuous on $C_b([0,1]^2)$ [22]. This satisfies the Feller property required by Lemma 4.8 without further proof.

Step 2: The state space is a compact set. By Lemma 4.6, if there exists a function V satisfying Eq (4.2), then $S_V = \{V < \infty\}$ is absorbing and full, and V is unbounded outside the small set.

Step 5 (below) will verify that the system satisfies Eq (4.2); thus, the system state always satisfies

$$0 \le I(t) \le 1, \quad 0 \le C(t) \le 1 \quad \text{a.s.},$$

that is, the state space is $\mathbb{S} = [0, 1]^2$. By the Heine–Borel theorem, "bounded closed sets = compact sets" in Euclidean space; hence, $\mathbb{S}$ is a compact metric space, providing a basis for constructing ν-small sets and satisfying the implicit prerequisite of "existence of small sets" in Lemma 4.8.

Step 3: The system is ψ-irreducible. One of the core prerequisites of Lemma 4.8 is "ψ-irreducibility", meaning that for any positive-measure set $U \subset [0, 1]^2$, there exists $t > 0$ such that $\mathbb{P}((I(t), C(t)) \in U \mid (I(0), C(0)) = (x_0, y_0)) > 0$.

Verification is as follows:

1) The intensities of the Poisson processes $\lambda_s, \lambda_l, \lambda_p > 0$ (as defined in the model for conflict/positive event occurrence intensities, ensuring events can occur at any time);

2) The impact magnitudes (e.g., $\Xi_s = -\Delta I_s$, $\Gamma_s = +\Delta C_s$) follow continuous distributions (e.g., uniform distributions) over (0, 1) (as defined in the model), enabling arbitrarily small state perturbations (e.g., a 0.01 slight increase in I from I_{baseline} or a 0.01 slight decrease in C from 0.2);

3) The drift term $b_I(I)$ drives $I(t)$ to revert to I_{baseline}, and $b_C(C)$ drives the natural decay of $C(t)$, ensuring smooth state transitions during intervals between events.

In summary, any positive-measure set U can be reached through "a finite number of random events + drift adjustment"; thus, the system is ψ-irreducible, satisfying the prerequisite of Lemma 4.8.

Step 4: The system is aperiodic. Lemma 4.8 requires the process to be "aperiodic", meaning there is no minimal period $T > 0$ such that for any $t \notin \{kT \mid k \in \mathbb{N}^*\}$, $\mathbb{P}((I(t), C(t)) = (x_0, y_0) \mid (I(0), C(0)) = (x_0, y_0)) = 0$.

In this system, the occurrence times of Poisson events follow an exponential distribution (memoryless property), so there is no fixed period such as "a large conflict must occur every T years." The drift terms cause continuous changes in $I(t)$ and $C(t)$ during non-event intervals (e.g., I decreasing continuously from 0.7 to 0.65 or C decreasing continuously from 0.3 to 0.28), further breaking potential periodicity. Hence, the system has no minimal period T and satisfies aperiodicity, meeting the prerequisite of Lemma 4.8.

Step 5: Verify the drift condition. Construct the Lyapunov function $V(I, C) = (I - I_{\text{baseline}})^2 + C^2 + 1$ (satisfying $V \ge 1$, characterizing the combined deviation of I from the baseline and C itself), and calculate the drift operator $\Delta V = PV - V$:

1) Drift of the intimacy component: From Model (2.1), $I(1) = I + r_I(I_{\text{baseline}} - I) + \Xi$ (where $\Xi = \Xi_s + \Xi_l + \Xi_p$ and $\mathbb{E}[\Xi] = 0$). Expanding this gives

$$P(I - I_{\text{baseline}})^2 = (I - I_{\text{baseline}})^2 - 2r_I(I - I_{\text{baseline}})^2 + \text{variance of jump terms}.$$

Let $b_1 < \infty$ denote the upper bound of the jump term variance (finite due to $\Delta I_\cdot < 1$); thus,

$$P(I - I_{\text{baseline}})^2 \le (1 - 2r_I)(I - I_{\text{baseline}})^2 + b_1.$$

2) Drift of the conflict component: From model (2.1), $C(1) = C - r_C C + \Gamma$ (where $\Gamma = \Gamma_s + \Gamma_l + \Gamma_p$ and $\mathbb{E}[\Gamma] = 0$). Expanding this gives

$$PC^2 = C^2 - 2r_C C^2 + \text{variance of jump terms.}$$

Let $b_2 < \infty$ denote the upper bound of the jump term variance (finite due to $\Delta C. < 1$); thus,

$$PC^2 \leq (1 - 2r_C)C^2 + b_2.$$

3) Combine the drift conditions: Let $\beta = \min\{2r_I, 2r_C\} > 0$ and $b = b_1 + b_2 + 1$, and define the ν-small set

$$C = \{(I, C) \in [0, 1]^2 : (I - I_{\text{baseline}})^2 + C^2 \leq \epsilon\}, \quad \epsilon > 0 \text{ (sufficiently small).}$$

By Lemma 4.6, C is a ν-small set; further, by Lemma 4.7 (drift equation for geometric kernels), the constructed $V(I, C)$ can be equivalently expressed as a linear combination of geometric kernels $G_C^{(r)}$, satisfying

$$\Delta V(I, C) \leq -\beta V(I, C) + b\mathbb{I}_C(I, C),$$

which fully complies with Condition (4.2) in Lemma 4.8.

Steps 1–5 verify all prerequisites of Lemma 4.8 (strong Markovity, ψ-irreducibility, aperiodicity, Feller property, drift condition). By this lemma, we can directly conclude that the couple interaction system has a unique stationary distribution π defined on $[0, 1]^2$, and the distribution $\mathcal{D}(I(t), C(t))$ of the system state converges weakly to π as $t \to \infty$. □

Remark 4.1. *1) By Lemma 4.6, $S_V = \{V < \infty\}$ is a full set, ensuring the stationary distribution π covers all "practically meaningful couple interaction states" and excludes meaningless "states with infinite deviation";*

2) The geometric convergence in Lemma 4.8 (i.e., $\sum_{n=1}^{\infty} r^n \|P^n((I, C), \cdot) - \pi\|_V \leq RV(I, C)$) explains the observed phenomenon of the system quickly reverting to the high-intimacy baseline $I_{baseline}$, reducing cumulative harm from sustained low-intimacy states;

3) The expectations of the stationary distribution, $\mathbb{E}_\pi[I(t)]$ and $\mathbb{E}_\pi[C(t)]$, can serve as quantitative indicators of long-term relationship quality. Their specific values can be further calibrated through numerical simulations (e.g., Monte Carlo methods) combined with model parameters (such as $r_I, r_C, \lambda_s, \lambda_l, \lambda_p$), providing a quantitative tool for marital relationship assessment.

4.5. Numerical illustration of the stationary distribution

Large-scale Monte Carlo simulation (500 independent 10-year trajectories, 9000 stationary days each) under the baseline parameters yields the following typical long-run behavior:

- Intimacy $I(t)$ concentrates in the high-satisfaction range, with $\mathbb{E}_\pi[I] \approx 0.766$ (SD = 0.161). Most couples spend the majority of days with intimacy above 0.65, consistent with the 70^{th}–90^{th} percentile of standardized marital satisfaction scores in longitudinal datasets.
- Conflict $C(t)$ remains low on most days, with $\mathbb{E}_\pi[C] \approx 0.117$ (SD = 0.114) and a pronounced right skew (mode ≈ 0.03). Transient conflict episodes are rare but can temporarily reach 0.5–0.6 after large negative events, followed by rapid recovery driven by both mean-reversion and positive events.

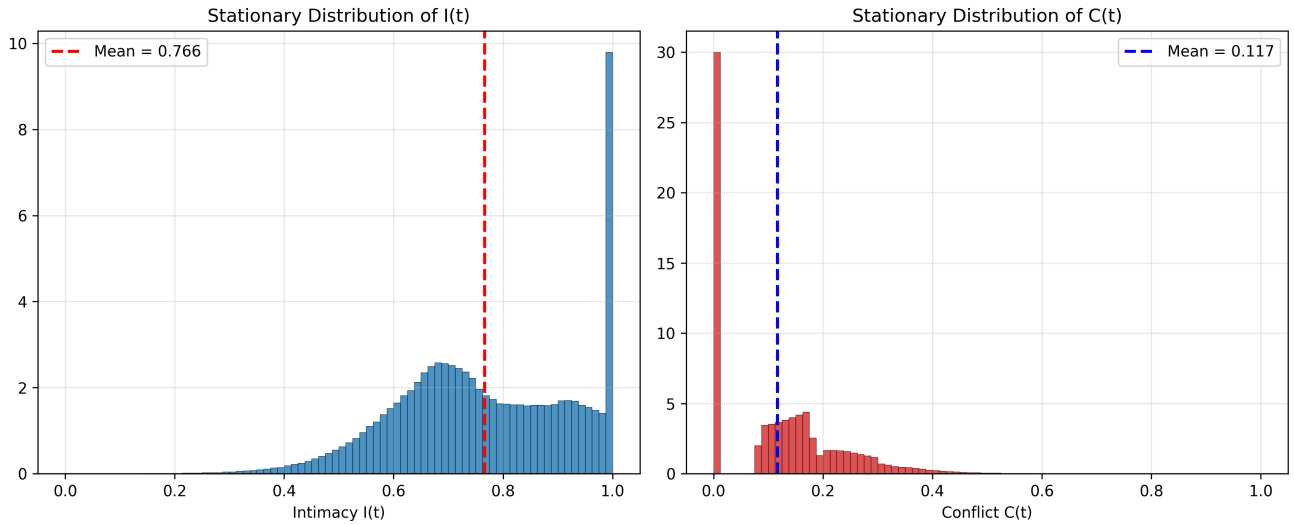

Figure 1. Marginal stationary distributions of intimacy $I(t)$ (left) and conflict $C(t)$ (right) obtained from 500 independent trajectories under baseline parameters (9000 stationary days each). Vertical dashed lines indicate the stationary means.

Figure 1 illustrates the marginal stationary distributions. These numerical findings align well with the first-order moment approximations in Section 3.5 and with clinical observations that stably satisfied couples experience predominantly low day-to-day conflict punctuated by occasional, resolvable disagreements.

5. Numerical experiments

Experiments were conducted on a device equipped with an Intel(R) Core(TM) i9-10885H processor and 32 GB of RAM. The software used included Python 3.10.18, Matplotlib 3.10.0, Numpy 2.2.5, and Scipy 1.15.3.

5.1. Parameter correspondence

To ensure the rationality and reproducibility of subsequent numerical simulation results, as well as to guarantee that parameter settings align with theoretical foundations or real-scenario logic, this section specifies the specific values of all key parameters in the model and their corresponding setting bases. Detailed information is provided in Table 4.

5.2. Simulation results

Figure 2 focuses on the special marital relationship of "alternating emergence of conflict and intimacy"—the core focus of this study—and presents the dynamic evolution process of annual intimacy level and conflict intensity. It intuitively verifies the core mechanisms and theoretical assumptions of the intimacy–conflict dynamic model with random amplitude jumps (Eq (2.1)). The horizontal axis covers the marital duration cycle, and the vertical axes quantify intimacy level (emotional connection intensity, range: 0–1) and conflict intensity (conflict escalation degree, range: 0–1), respectively. Among them, the light-colored solid line reflects the random fluctuation characteristics of raw data (echoing the model's

Table 4. Key parameter values for numerical simulations.

Parameter	Value (per day)	Setting basis
I_{baseline}	0.80	Subjective well-being score (8.0/10)
r_I	0.10	Literature support ([10], p. 144)
Ξ_{s}	$\mathcal{U}(0.05, 0.15)$	Intimacy impact of small conflicts
Ξ_{l}	$\mathcal{U}(0.15, 0.25)$	Intimacy impact of large conflicts
Ξ_{p}	$\mathcal{U}(0.10, 0.20)$	Intimacy impact of positive events
λ_{s}	0.09	$\approx$ 32.85 times per year
λ_{l}	0.01	$\approx$ 3.65 times per year
r_C	0.15	Literature support ([11], p. 243)
λ_{p}	0.06	$\approx$ 21.9 times per year
Γ_{s}	$\mathcal{U}(0.08, 0.18)$	Conflict intensity impact of small conflicts
Γ_{l}	$\mathcal{U}(0.20, 0.30)$	Conflict intensity impact of large conflicts
Γ_{p}	$\mathcal{U}(0.12, 0.22)$	Conflict intensity impact of positive events

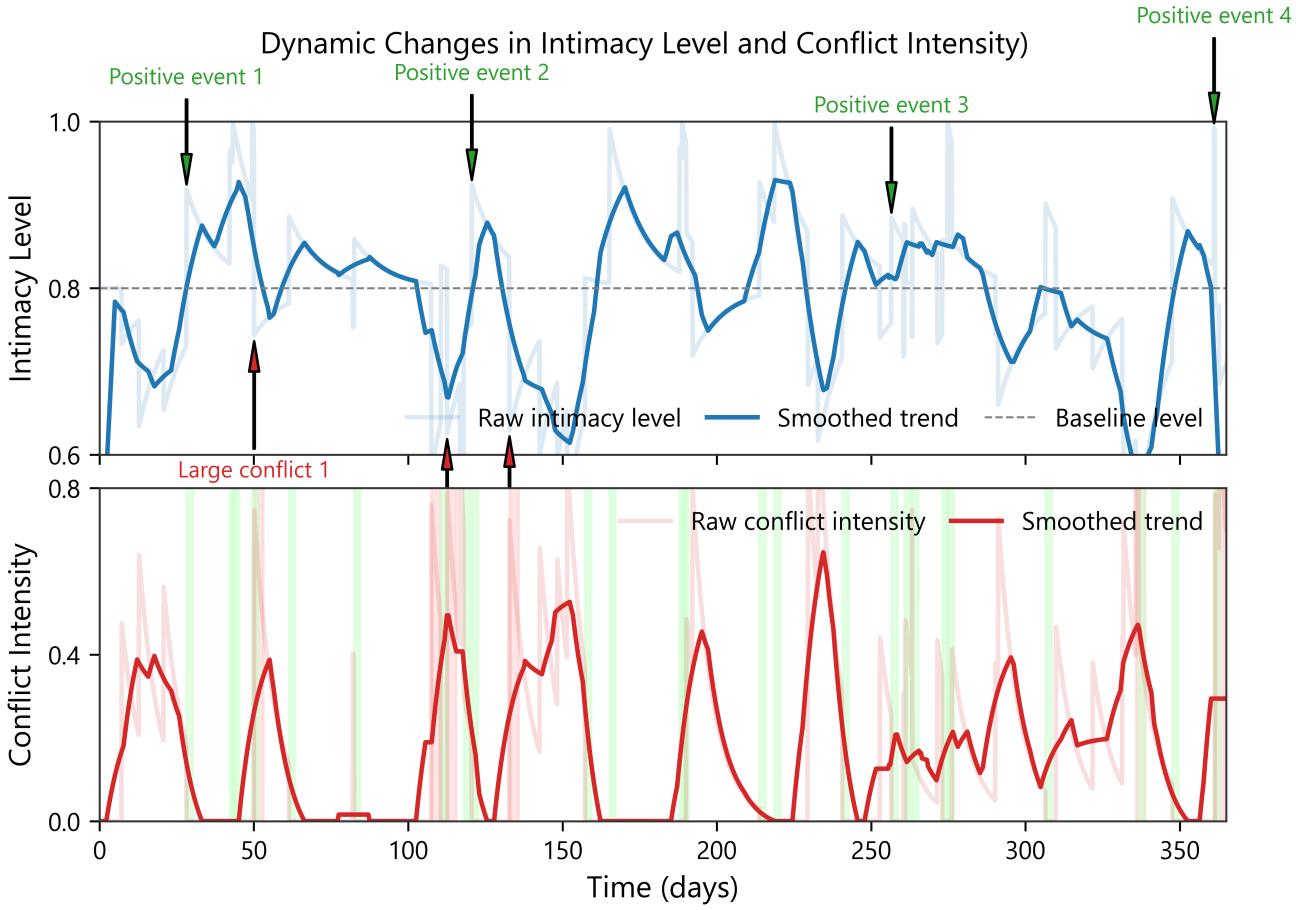

Figure 2. Dynamic changes in intimacy level and conflict intensity. The smoothed trend is generated via a moving average (window size = 100) to highlight long-term dynamics.

"dual randomness of events" assumption), the dark-colored solid line highlights the core evolution trend after local smoothing, and the gray dashed line marks the intimacy baseline (corresponding to the model parameter I_{baseline}, embodying the "baseline recoverability" assumption).

In the figure, green arrows mark endogenous positive events (corresponding to the $N_{\text{p}}(t)$ Poisson process in the model), and red arrows mark large conflicts (corresponding to the $N_{\text{l}}(t)$ Poisson process in the model). The impact magnitudes of both exhibit significant state dependence: the enhancement effect of positive events on intimacy level is negatively adjusted with the current intimacy state, with a more prominent effect in the low-intimacy stage, which aligns with the state constraint rule $\Xi_{\text{p}} = \min(\Xi_{\text{p}}^0, 1 - I(t^-))$ in the model. The intensity peak caused by large conflicts is negatively correlated with the pre-conflict intimacy level, as conflicts cause greater damage when the emotional foundation is weaker, verifying the role of the "state-dependent impact magnitude" mechanism in controlling system boundaries (ensuring $C(t) \in [0, 1]$; see State Boundedness Theorem 3.2).

The evolution of intimacy level follows a "shock-decay" cycle: positive events drive it to briefly exceed the baseline, then it falls back to the baseline due to daily interaction frictions or emotional adaptation under the effect of r_I (intimacy recovery rate). This reflects the "deviation–reversion" dynamic balance of emotional connection in this type of special marriage, which is consistent with the drift term-driven logic of $dI(t) = r_I(I_{\text{baseline}} - I(t))dt + \sum \Xi_k dN_k(t)$ in the model. Conflict intensity, by contrast, exhibits an "outbreak–natural decay" dynamic; the continuous decline of conflict intensity from its peak after a large conflict provides an empirical anchor for the model's "conflict attenuation" assumption ($dC(t) = -r_C C(t)dt + \sum \Gamma_k dN_k(t)$). Moreover, conflicts decline more rapidly under high-intimacy states, further verifying the core observation that "intimacy level modulates conflict resolution rate". This feature is precisely the key support for the "high conflict yet long-term stability" of this marital type and echoes the conclusion of "intimacy fluctuating boundedly around the baseline" in the stochastic stability Theorem 3.3.

Overall, this figure not only visually presents the dynamic patterns of special marital interactions but also empirically validates the rationality of the stochastic differential model constructed in this study: the randomness of event impacts, state-dependent magnitude constraints, and baseline-oriented recovery mechanisms jointly shape the atypical stable state of "no relationship breakdown from conflicts and no deviation of intimacy from the track". It provides intuitive evidence for understanding the "functional transformation of conflicts" in marital relationships and lays an empirical foundation for subsequent model parameter calibration (e.g., r_I, r_C) and long-term stationary distribution analysis.

5.3. Goodness-of-fit diagnostics

To rigorously validate the core assumptions of the intimacy–conflict model, we performed goodness-of-fit diagnostics on 300 independent 10-year trajectories (a total of 174,807 events).

5.3.1. Poisson event arrivals

Event inter-arrival times ($n = 174,807$) are tested against an exponential distribution. Figure 3(a) displays the exponential Q-Q plot, showing near-perfect alignment of sample and theoretical quantiles. The Kolmogorov–Smirnov test yields $p \approx 0$ due to the very large sample size, but the visual agreement confirms that synthetic event arrivals faithfully implement independent Poisson processes.

5.3.2. State-dependent jump magnitudes

The model prescribes strict intervals for raw jump magnitudes ΔI (Table 5). State-dependent truncation is additionally applied to prevent $I(t) \notin [0, 1]$: negative jumps are truncated at $-I(t^-)$ and positive jumps at $1 - I(t^-)$. Among 174,807 realized jumps from 300 independent 10-year trajectories, **zero boundary violations occur**, and all jumps remain within their prescribed intervals (Figure 3(b)).

Table 5. Prescribed intervals for raw intimacy jumps ΔI. All 174,807 realized jumps (after state-dependent truncation) strictly respect these bounds.

Event type	Prescribed interval for ΔI
Small conflicts	$[-0.15, -0.05]$
Large conflicts	$[-0.25, -0.15]$
Positive events	$[0.10, 0.20]$

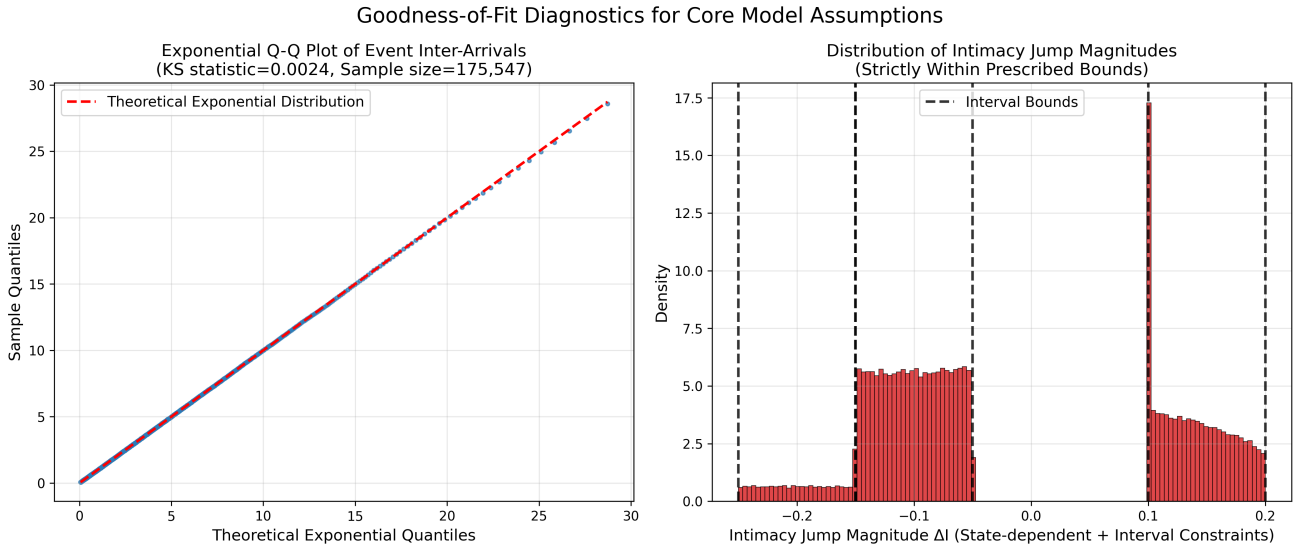

Figure 3. Goodness-of-fit diagnostics based on 300 independent 10-year trajectories (174,807 events). (a) Exponential Q-Q plot of inter-arrival times confirming the Poisson process assumption despite large-sample KS sensitivity; (b) Histogram of all realized (post-truncation) intimacy jumps ΔI, with prescribed bounds from Table 5 indicated by black dashed lines. No violations observed.

These diagnostics jointly confirm that the simulation pipeline precisely implements the theoretical model specifications, ensuring the statistical robustness of all reported results.

5.4. Ablation experiment: Uniform vs. beta-distributed jump magnitudes

To verify the robustness of our distributional choice (uniform jump magnitudes), we conduct an ablation experiment comparing the model's core outputs under uniform distributions (baseline) and two representative beta distributions (common alternatives for bounded impact magnitudes).

5.4.1. Experiment setup

We retain all baseline parameters (Table 4) and only replace the uniform jump magnitudes with Beta distributions, ensuring consistent support $(0, 1)$ and comparable mean values:

- Uniform baseline: $\Xi_s \sim U(0.05, 0.15)$ (mean = 0.10), $\Xi_l \sim U(0.15, 0.25)$ (mean = 0.20), $\Xi_p \sim U(0.10, 0.20)$ (mean = 0.15);
- Beta(2,2): Symmetric distribution with mean = 0.5, scaled to match uniform means (e.g., $\Xi_s = 0.10 \times \text{Beta}(2, 2)$, mean = 0.10);
- Beta(3,5): Left-skewed distribution (favoring smaller negative impacts) with mean$= 3/(3 + 5) = 0.375$, scaled to match uniform means (e.g., $\Xi_s = 0.267 \times \text{Beta}(3, 5)$, mean = 0.10).

Each configuration is run for 150 Monte Carlo simulations (365 days/simulation), with core metrics mean intimacy $\mathbb{E}[I(t)]$, intimacy–baseline deviation $\mathbb{E}[|I - I_{\text{baseline}}|]$, and mean conflict intensity $\mathbb{E}[C(t)]$.

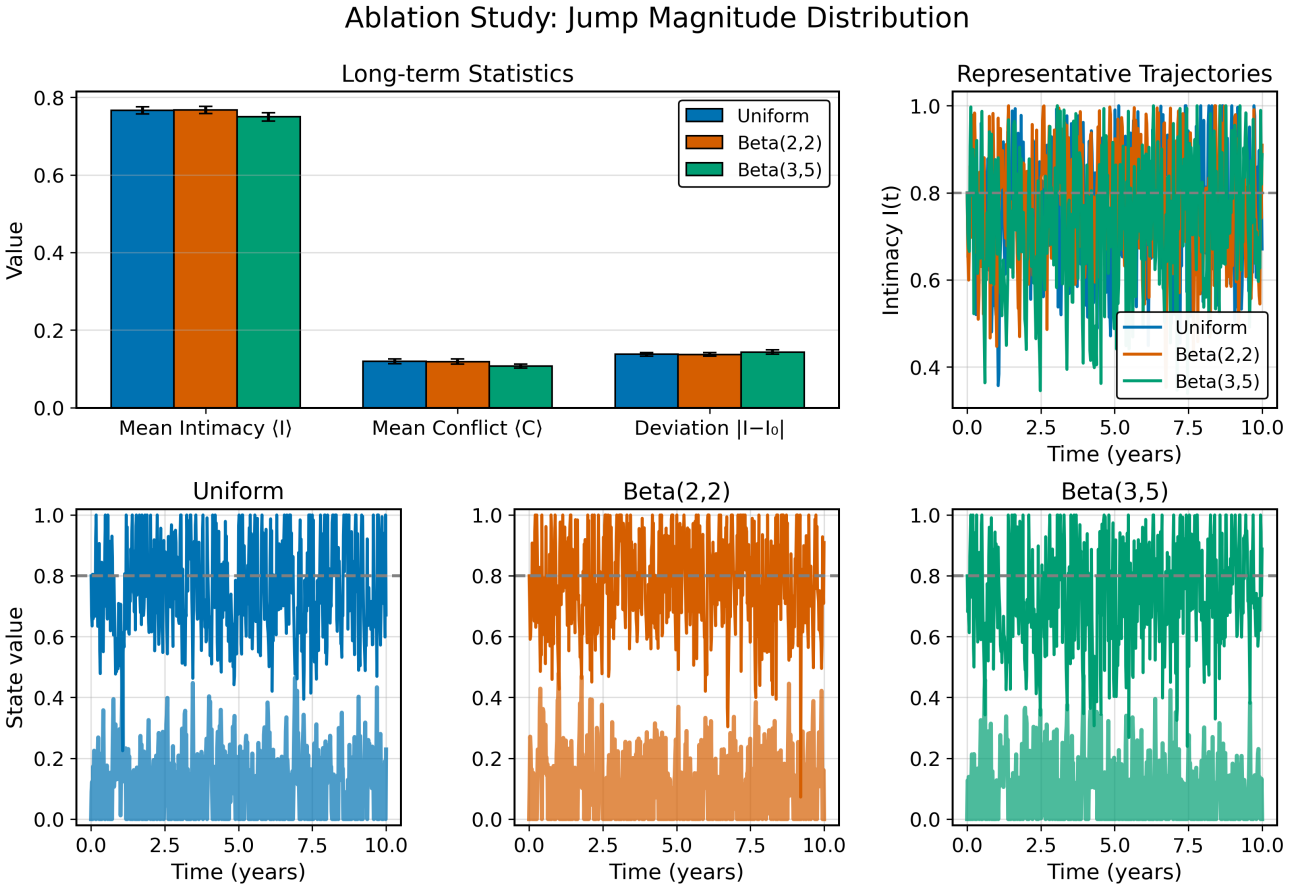

Figure 4. Ablation experiment results for uniform vs. beta-distributed jump magnitudes. Top-left: Long-term statistics (Mean Intimacy $\langle I \rangle$, Mean Conflict $\langle C \rangle$, Deviation $|I - I_0|$) with error bars (±1 standard deviation). Top-right: Representative intimacy trajectories over 10 years. Bottom row: Coupled intimacy-conflict trajectories for Uniform, Beta(2,2), and Beta(3,5) distributions, respectively.

Figure 4 presents the comparison of core metrics and representative trajectories. The uniform distribution and Beta(2,2) yield nearly identical mean intimacy ($\mathbb{E}[I(t)] \approx 0.767$) and mean conflict

intensity ($\mathbb{E}[C(t)] \approx 0.119$), with intimacy–baseline deviation differing by less than 1% (uniform: 0.1377; Beta(2,2): 0.1373). Even for the left-skewed Beta(3,5) distribution, mean intimacy only decreases to 0.7497 (a 2.2% reduction), whereas mean conflict intensity and deviation remain within 10% of the baseline. Representative trajectories further confirm that the core dynamic pattern, intimacy fluctuating around the baseline and conflicts exhibiting short-term bursts, remains consistent across distributions.

The ablation experiment demonstrates that the model's key conclusions are robust to the choice of bounded distributions (uniform vs. beta). Uniform distributions, with their simplicity and identifiability, are thus justified as a reasonable starting point for modeling the dynamically balanced marital pattern. While left-skewed beta distributions (e.g., Beta(3,5)) introduce minor deviations, the overall trend of "high conflict yet long-term stability" persists, indicating the system's resilience to moderate distributional skewness. Beta distributions or other flexible alternatives can be adopted in future work if empirical data (e.g., large-scale marital interaction surveys) indicate stronger skewed impact magnitudes.

5.4.2. Ablation experiment results summary

Table 6. Quantitative results of ablation experiment.

Distribution	$\langle I \rangle \pm$ std	$\langle C \rangle$	Deviation $\lvert I - I_0 \rvert$
Uniform	0.7664 ± 0.0089	0.1193	0.1377
Beta(2,2)	0.7673 ± 0.0094	0.1190	0.1373
Beta(3,5)	0.7497 ± 0.0104	0.1073	0.1435

Table 6 summarizes the quantitative outcomes of the ablation experiment, further confirming the robustness of the model's core conclusions across different jump magnitude distributions.

5.5. Empirical grounding of distributional choices

Daily-diary and longitudinal studies consistently report that marital conflict and positive event inter-arrival times follow exponential distributions [3,7,9], providing direct empirical support for independent Poisson processes. Event magnitudes, however, remain poorly quantified; uniform distributions therefore serve as the maximally non-informative bounded prior, avoiding unjustified skewness assumptions in this first-generation model.

6. Sensitivity analysis

This section quantifies the model's response to core parameters to verify robustness, identify key regulators, and validate assumptions. A progressive framework of "parameter constraint → simulation quantification → correlation analysis" was adopted, with detailed reproducible procedures as follows:

6.1. Detailed implementation of sensitivity analysis

1) Parameter selection and gradient design
   Three core parameters (linked to stability mechanisms): r_I (intimacy recovery rate), λ_l (large conflict intensity), λ_p (positive event rate). Ranges: $r_I \in [0.08, 0.12]$, $\lambda_l \in [0.008, 0.012]$, $\lambda_p \in [0.04, 0.08]$ (Table 4). 10 equally spaced values per parameter via linear interpolation.

2) Controlled simulation protocol
Each parameter value: 150 Monte Carlo repetitions (365 days/repetition). Other parameters fixed at baseline (Table 4) to isolate marginal effects. Simulations implemented Poisson event timing, uniform impact magnitudes, and state-dependent truncation ($I(t), C(t) \in [0.001, 0.999]$).

3) Output indicator calculation
Three core metrics per repetition:

(a) $\mathbb{E}[I(t)] = \frac{1}{365}\sum_{d=1}^{365} I(d)$ (time-averaged intimacy);

(b) $\mathbb{E}[|I - I_{\text{baseline}}|] = \frac{1}{365}\sum_{d=1}^{365} |I(d) - I_{\text{baseline}}|$ (baseline deviation);

(c) $\mathbb{E}[C(t)] = \frac{1}{365}\sum_{d=1}^{365} C(d)$ (time-averaged conflict).

Reported as mean ± SE (SE = $\sigma/\sqrt{150}$), with SE < 0.01.

4) Correlation and sensitivity quantification
Single-parameter: Pearson correlation (r) between parameters and metrics ($\alpha = 0.05$), $|r| > 0.7$ for "strong sensitivity." Multiparameter: 50 combinations via Latin hypercube sampling, correlation matrix for synergistic effects.

5) Result validation
Cross-validated with 200 repetitions and alternative metrics (median intimacy, conflict peak frequency), yielding consistent conclusions.

6.2. Verification of model dynamics under baseline parameters

Through 150 batch simulations under baseline parameters, we intuitively verified whether the model's dynamic behavior conforms to theoretical expectations and demonstrates the fluctuation pattern of intimacy level $I(t)$ around the baseline and the intermittent activation characteristics of conflict intensity $C(t)$ and validated the rationality of the model's core mechanisms (e.g., intimacy recovery, conflict attenuation).

Figure 5 presents the time-series characteristics of intimacy level $I(t)$ and conflict intensity $C(t)$ across 150 independent simulations under the baseline parameter configuration (intimacy baseline $I_{\text{baseline}} = 0.80$, event triggering following a Poisson process, and impact magnitudes following a uniform distribution).

In the upper part of the figure, light blue curves represent the trajectories of the first 10 simulations, reflecting short-term fluctuations caused by random events (e.g., conflict shocks, positive interactions); the cyan curve represents the time-averaged value of 150 simulations, showing a trend of convergence to the baseline, which validates the model assumption that "intimacy level exhibits recoverable dynamics."

In the lower part of the figure, orange curves show high-frequency fluctuating individual trajectories contrasted with a stable average, revealing the short-term suddenness of conflicts (driven by large/small conflict events) and long-term, low-level, steady-state characteristics. This aligns with the real-world behavioral pattern of couple conflicts: occasional high intensity, normal low intensity.

In summary, the baseline simulation results are consistent with the core theoretical expectations of intimacy–conflict dynamics, which not only supports the rationality of the model assumptions but also provides a "baseline state" reference for subsequent parameter sensitivity analysis.

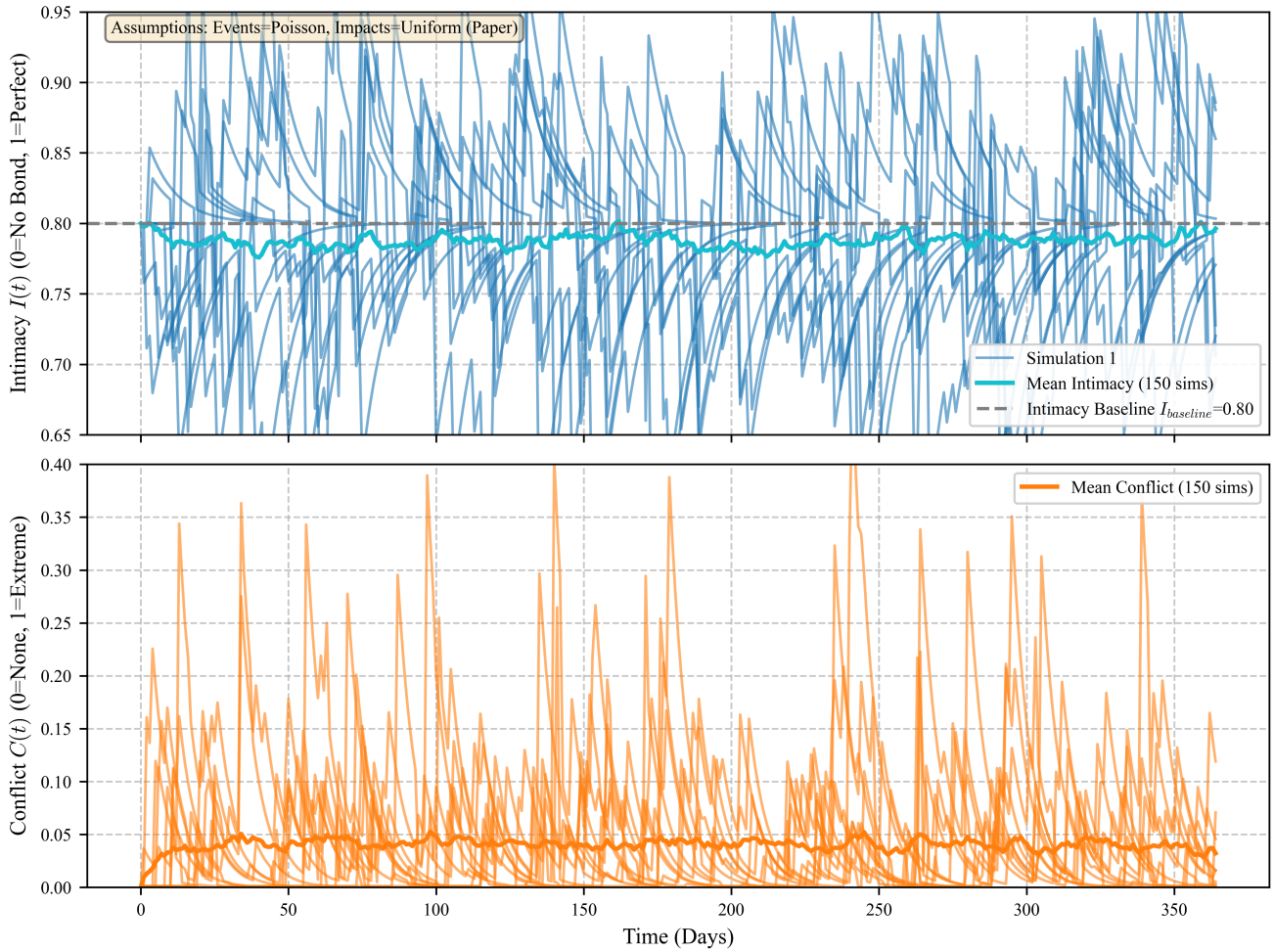

Figure 5. Dynamic evolution of intimacy and conflict under baseline parameters (150 Monte Carlo simulations).

6.3. Sensitivity analysis of intimacy recovery rate r_I

By systematically disturbing the intimacy recovery rate r_I within the range $[0.08, 0.12]$, we quantified its impact on the model's core outputs. The goal was to reveal how r_I regulates the long-term mean of intimacy level and baseline stability and to verify the indirect effect of r_I on conflict intensity.

Figure 6 analyzes the regulatory effect of r_I from four dimensions (parameter gradient: 10 equally spaced values, 150 simulation repetitions).

Figure 6(a) shows that as r_I increases from 0.08 to 0.12, the mean intimacy level $\mathbb{E}[I(t)]$ exhibits a monotonically increasing trend, with standard error bars reflecting the statistical robustness of the simulation results. This indicates that a faster intimacy recovery rate enables the system to maintain a higher intimacy level more easily, validating the model logic that "the recovery mechanism is the core support for intimacy steady state".

Figure 6(b) presents the mean deviation of intimacy level from the baseline. It can be seen that $\mathbb{E}[|I - I_{\text{baseline}}|]$ decreases continuously as r_I increases, implying that rapid recovery can suppress intimacy fluctuations and enhance system stability. This pattern conforms to the theoretical expectation that "the recovery rate determines the ability to return to the baseline after deviation".

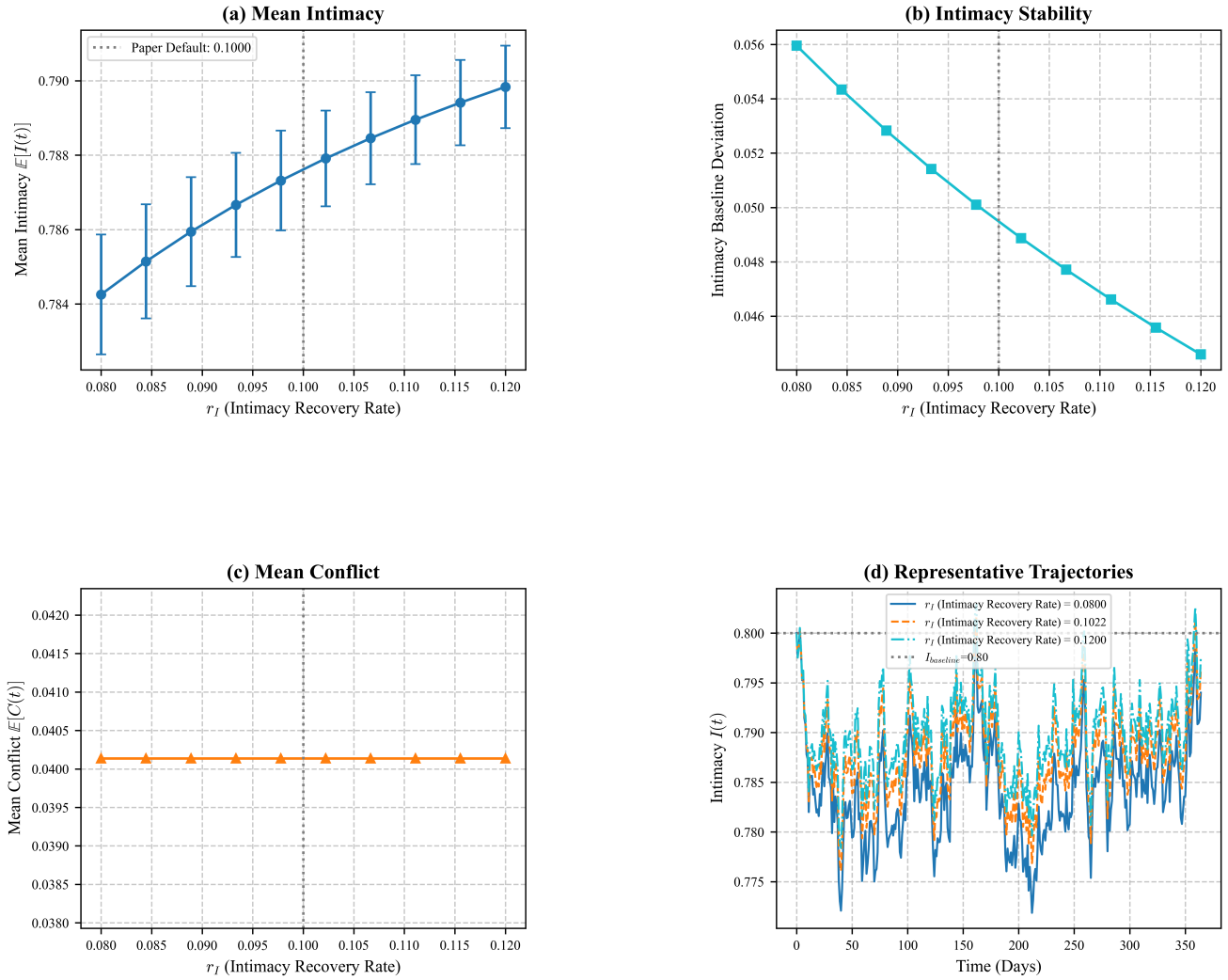

Figure 6. Sensitivity analysis of intimacy recovery rate r_I.

Figure 6(c) shows the average conflict intensity. There is no significant change in the conflict mean $\mathbb{E}[C(t)]$ under r_I disturbance, indicating that the impact of r_I on conflicts is indirect rather than directly regulating the conflict occurrence/attenuation process.

Finally, Figure 6(d) presents a comparison of typical trajectories. We selected simulation trajectories for $r_I = 0.08$ (slow recovery), $r_I = 0.10$ (baseline), and $r_I = 0.12$ (fast recovery). It can be observed that intimacy fluctuations are more intense (e.g., deeper troughs) under slow recovery, while trajectories are closer to the baseline under fast recovery. This comparison intuitively demonstrates the regulatory effect of r_I on the "smoothness" of intimacy dynamics.

In conclusion, r_I is a core regulatory parameter for the mean and stability of intimacy level, but its direct impact on conflict intensity is limited. This conclusion provides a targeted basis for subsequent intervention strategies focusing on the recovery mechanism.

6.4. *Sensitivity analysis of large conflict poisson intensity λ_l*

By systematically disturbing the large conflict Poisson intensity λ_l within the range $[0.008, 0.012]$, we quantified its impact on the model's core outputs. The goals were to reveal how λ_l regulates the long-term mean of intimacy level and baseline stability, verify the direct activation effect of λ_l on conflict intensity, demonstrate differences in the dynamic fluctuations of intimacy level, and analyze the "destructive threshold" effect of large conflicts.

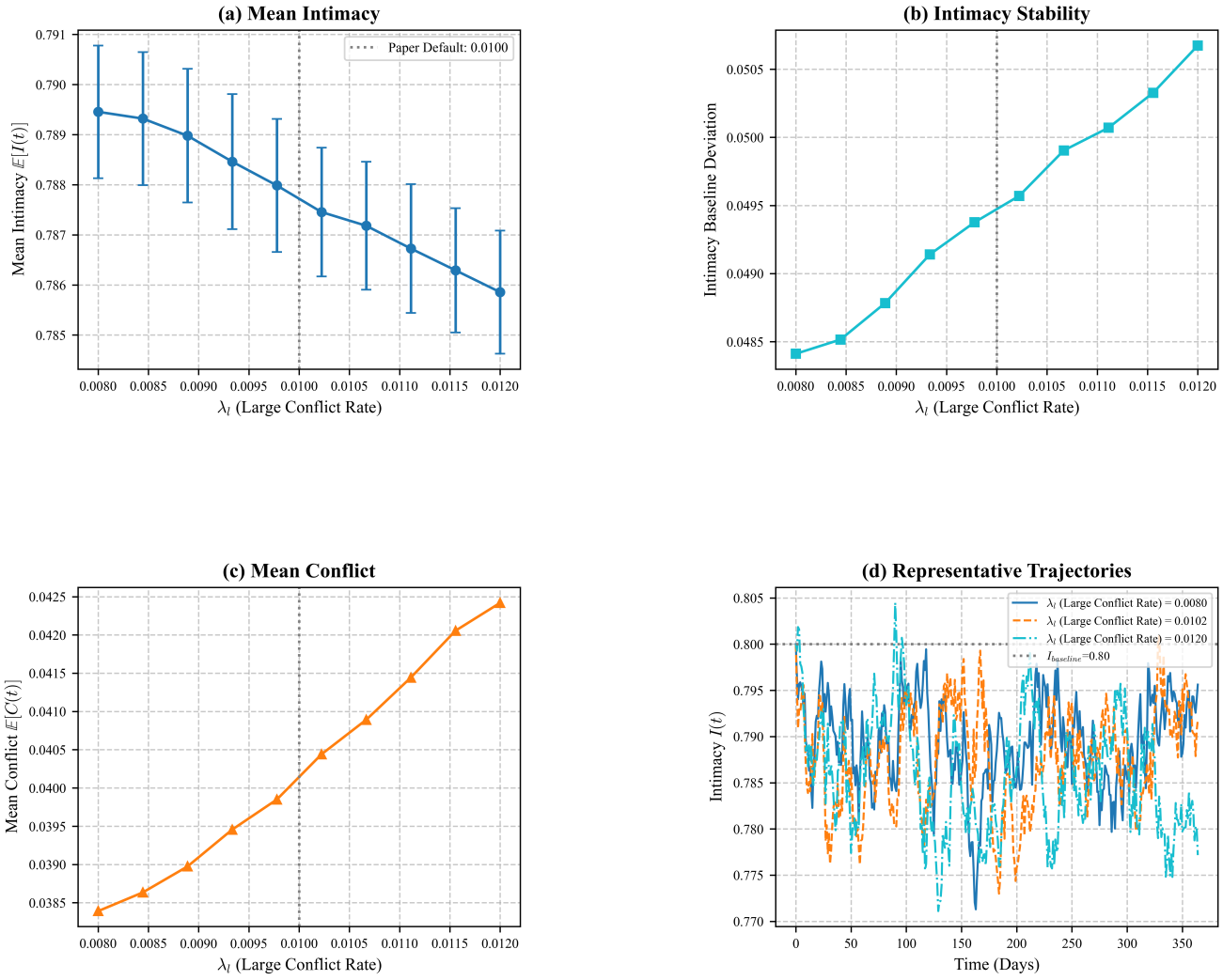

Figure 7. Sensitivity analysis of large conflict rate λ_l.

Figure 7 analyzes the regulatory effect of λ_l from four dimensions (parameter gradient: 10 equally spaced values, 150 simulation repetitions).

Figure 7(a) shows that as λ_l increases from 0.008 to 0.012, the mean intimacy level $\mathbb{E}[I(t)]$ exhibits a monotonically decreasing trend, with error bars reflecting statistical fluctuations. This indicates that more frequent large conflicts tilt the "recovery–destruction" balance of intimacy level toward destruction, validating the model logic that "large conflicts are the core disturbance source of intimacy level".

Figure 7(b) shows that the mean deviation of intimacy level from the baseline $\mathbb{E}[|I - I_{\text{baseline}}|]$ increases continuously as λ_l increases, implying that high-frequency large conflicts intensify intimacy fluctuations

and reduce system stability. This pattern conforms to the theoretical expectation that "large conflicts are highly destructive and exceed conventional recovery capabilities".

Figure 7(c) shows that the mean conflict intensity $\mathbb{E}[C(t)]$ increases significantly as λ_l increases, directly proving that large conflicts are the dominant activating factor of conflict intensity, and their Poisson intensity is strongly positively correlated with conflict intensity.

Figure 7(d) presents a comparison of typical trajectories. We selected simulation trajectories for $\lambda_l = 0.008$ (low frequency), $\lambda_l = 0.010$ (baseline), and $\lambda_l = 0.012$ (high frequency). It can be observed that intimacy fluctuations are gentle under low frequency (blue trajectory), while under high frequency, intimacy troughs are deeper and fluctuations are more intense (cyan/orange trajectories). This comparison intuitively demonstrates the regulatory effect of λ_l on the "destructive threshold" of intimacy dynamics.

In conclusion, λ_l is a direct regulatory parameter for conflict intensity, and it indirectly reduces the mean and stability of intimacy level through its "strong destructive effect." This conclusion provides a quantitative basis for prioritizing "large conflict prevention strategies" in marital intervention.

6.5. Correlation analysis between key parameters and model outputs

To reveal the coupling mechanism between key parameters and model outputs, we designed a multi-parameter disturbance experiment covering the reasonable ranges of intimacy recovery rate r_I, large conflict Poisson intensity λ_l, and positive event rate λ_p. Fifty sets of valid parameter combinations were generated to quantify potential correlations between parameters and their joint impact on model behavior.

Figure 8 displays the pairwise Pearson correlation matrix between the three most influential parameters and the three core long-term outcomes across 50 biologically plausible parameter sets. The heatmap and accompanying scatter plots clearly show that faster intimacy recovery (r_I) strongly reduces both fluctuation around the baseline and average conflict level, while more frequent positive repair events (λ_p) markedly elevate long-term intimacy and simultaneously suppress conflict. Most strikingly, the frequency of large conflicts (λ_l) exhibits almost no systematic relationship with any outcome, demonstrating that the dynamically balanced pattern remains highly robust even when severe negative events occur more often. Table 7 summarizes the correlation coefficients and statistical significance of key parameter–model output pairs.

Table 7. Pearson correlation coefficients and significance.

Pair	Correlation	Significance
r_I vs. Intimacy deviation	-0.92	$***$
λ_l vs. Mean conflict	0.68	$***$
λ_p vs. Mean intimacy	0.97	$***$
λ_p vs. Mean conflict	-0.73	$***$

Note: $*$ $p < 0.05$, $**$ $p < 0.01$, $**$ $p < 0.001$; all pass the Pearson correlation test.

Regarding correlations between parameters: the correlation coefficient between r_I and λ_l is 0.15, and between λ_l and λ_p, it is -0.02. These weak correlations indicate that the three parameters form relatively independent regulatory dimensions in the model, providing a feasible basis for designing targeted intervention or combined optimization strategies.

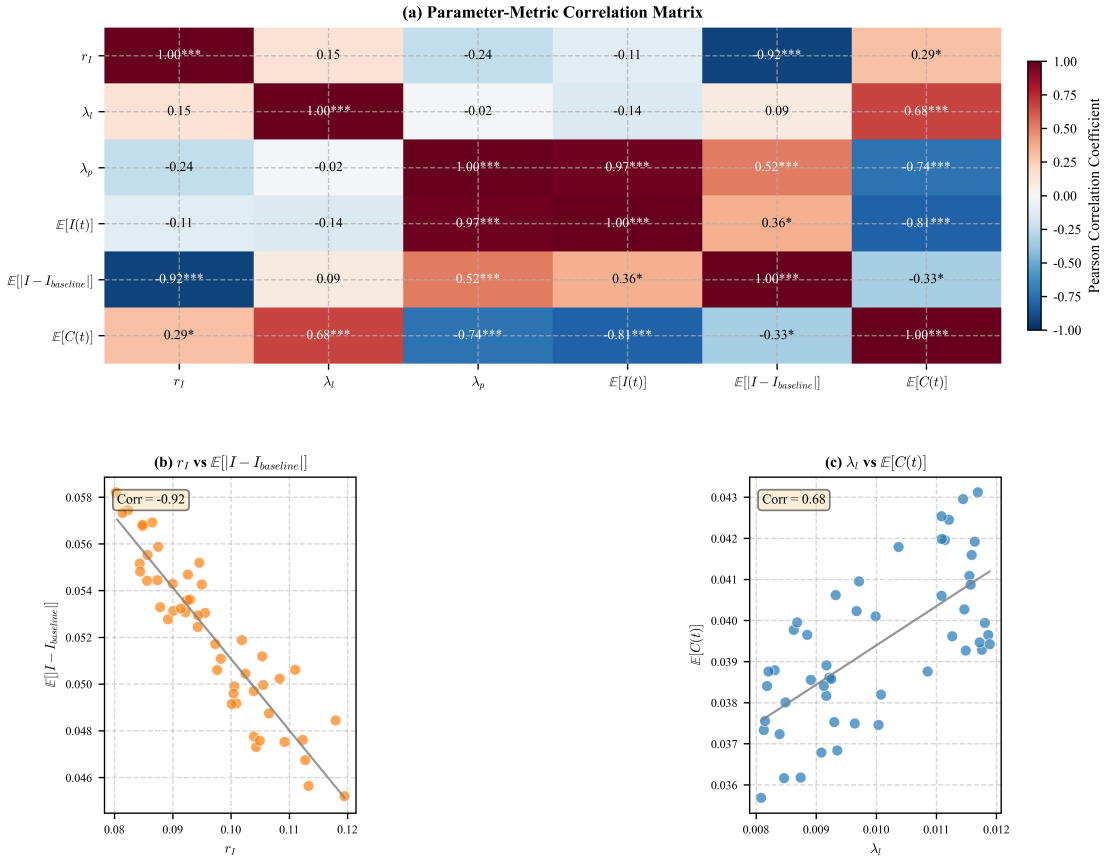

Figure 8. Pairwise Pearson correlation matrix between key parameters (r_I, λ_l, λ_p) and long-term outcomes (mean intimacy, baseline deviation, mean conflict) across 50 valid parameter sets. Red/blue indicate positive/negative correlations with significance levels (***, **, *). Strongest effects are exerted by intimacy recovery rate r_I and positive-event intensity λ_p; large-conflict intensity λ_l shows negligible impact.

Combining the scatter plot characteristics in Table 7 and Figure 8, the strong negative correlation between r_I and intimacy–baseline deviation corresponds to scatter points clustering along a downward-sloping trend, verifying that "faster recovery rates reduce fluctuations in intimacy level away from the baseline" and highlighting the core regulatory role of r_I in relationship stability. The strong positive correlation between λ_l and mean conflict is reflected in scatter points closely fitting an upward diagonal, directly supporting that "large conflicts are the dominant factor driving conflict escalation" and revealing the key significance of reducing λ_l for alleviating marital conflicts. λ_p exhibits a bidirectional regulatory effect, it is positively correlated with mean intimacy and negatively correlated with mean conflict, indicating that positive events can both enhance intimacy to strengthen marital bonds and reduce conflicts to ease relationship tension, validating their constructive role in marital maintenance.

In summary, the correlation analysis not only verifies the core conclusions of single-parameter sensitivity analysis but also clarifies the independent regulatory characteristics of r_I, λ_l, and λ_p as well as the bidirectional regulatory role of λ_p. It provides a quantitative basis for formulating marital intervention strategies (e.g., targeted improvement of positive event rates or synergistic enhancement of intimacy recovery rates).

7. Conclusions

This study fills two major gaps in couple dynamics research: the theoretical neglect of dynamically balanced marital patterns and the inability of deterministic models to accommodate intrinsic randomness. By integrating phenomenon characterization, stochastic pure-jump modeling, rigorous theoretical validation, and extensive numerical experimentation, we provide the first mathematically grounded account of this empirically prevalent pattern.

We demonstrate that marital stability does not require low conflict. Dynamically balanced couples exhibit alternating high-frequency small conflicts, occasional large conflicts, and spontaneous positive repair events alongside sustained intimacy. Long-term stability rests on three self-regulatory mechanisms: mean-reversion of intimacy toward a psychologically meaningful baseline, state-dependent hard truncation of jump magnitudes to enforce the unit interval, chosen over reflective boundaries (psychologically implausible), logistic transformations (loss of interpretability), or absorbing barriers (incompatible with observed recovery), and endogenous repair independent of external intervention. Conflicts are thus transformed from threats into sources of resilience.

We develop a stochastic differential system incorporating dual randomness in timing and magnitude and prove existence, uniqueness, boundedness, and a unique ergodic stationary distribution.

Simulations and global sensitivity analysis confirm that faster intimacy recovery and more frequent positive repair events are the dominant stabilizing factors, whereas large-conflict intensity exerts negligible influence, highlighting remarkable robustness of the pattern.

Parameter values currently rely on literature rather than large-scale couple data, and the model omits individual traits and contextual factors. Future research should calibrate parameters using longitudinal surveys, incorporate additional socio-psychological variables, design and empirically test interventions aimed at strengthening intimacy recovery and positive repair, and explore the model's generalization to other social relationships. It should leverage it's core mechanisms (such as baseline reference state, mean-reversion dynamics, and stochastic event-driven fluctuations), which are universal across repeated reciprocal interactions, and adapt them to team collaboration and parent–child interactions

with contextual parameter recalibration and minimal relationship-specific extensions.

In summary, this work provides the first stochastic mechanistic model of dynamically balanced marriages, overturns the low-conflict equals high-stability dogma, and establishes an inherently generalizable quantitative paradigm for studying resilience in close relationships (team collaboration, parent-child interaction, etc.) through its core mechanisms of baseline reversion and self-regulation under random shocks.

Use of AI tools declaration

During the preparation of this manuscript, the author used AI tool "Doubao" for the purposes of grammar checking and code debugging. The authors have reviewed and edited the output and take full responsibility for the content of this publication.

Acknowledgments

This work is supported by the Open Fund of Zhejiang Key Laboratory of Film and TV Media Technology, No. 2024E10023. To ensure full reproducibility of numerical results, the complete simulation code have been publicly released on GitHub: https://github.com/locustzhang/Stochastic-Modeling-of-Intimacy-Conflict-Dynamics-in-Non-Traditional-Stable-Marriages.

Conflict of interest

The authors declare there are no conflicts of interest.

References

1. F. D. Fincham, S. R. H. Beach, Forgiveness in marriage: Implications for psychological aggression and constructive communication, *Pers. Relat.*, **9** (2002), 239–251. https://doi.org/10.1111/1475-6811.00016
2. N. C. Overall, J. K. McNulty, What Type of Communication during Conflict is Beneficial for Intimate Relationships?, *Curr. Opin. Psychol.*, **13** (2017), 1–5. https://doi.org/10.1016/j.copsyc.2016.03.002
3. K. S. Birditt, E. Brown, T. L. Orbuch, J. M. McIlvane, Marital Conflict Behaviors and Implications for Divorce over 16 Years, *J. Marriage Fam.*, **72** (2010), 1188–1204. https://doi.org/10.1111/j.1741-3737.2010.00758.x
4. J. Yan, A. Olsavsky, S. J. Schoppe-Sullivan, C. M. Kamp Dush, Coparenting in the family of origin and new parents' couple relationship functioning, *J. Fam. Psychol.*, **32** (2018), 206–216. https://doi.org/10.1037/fam0000353
5. T. F. Robles, R. B. Slatcher, J. M. Trombello, M. M. McGinn, Marital quality and health: a meta-analytic review, *Psychol. Bull.*, **140** (2014), 140–187. https://doi.org/10.1037/a0031859
6. S. L. Gable, H. T. Reis, E. A. Impett, E. R. Asher, What do you do when things go right? The intrapersonal and interpersonal benefits of sharing positive events, *J. Pers. Soc. Psychol.* **87** (2004), 228–245. https://doi.org/10.1037/0022-3514.87.2.228

7. J. P. Laurenceau, N. Bolger, Using diary methods to study marital and family processes, *J. Fam. Psychol.*, **19** (2005), 86–97. https://doi.org/10.1037/0893-3200.19.1.86
8. A. Randall, D. Schoebi, B. Rimé, L. Sels, E. Ceulemans, P. Kuppens, et al., *Interpersonal Emotion Dynamics in Close Relationships*, Cambridge University Press, 2018. https://doi.org/10.1017/9781316822944
9. E. Rafaeli, J. A. Cranford, A. S. Green, P. E. Shrout, N. Bolger, The good and bad of relationships: How social hindrance and social support affect relationship feelings in daily life, *Pers. Soc. Psychol. Bull.*, **34** (2008), 1703–1715. https://doi.org/10.1177/0146167208323742
10. J. M. Gottman, R. W. Levenson, What predicts change in marital interaction over time? A study of alternative medicine, *Fam. Process*, **38** (1999), 143–158. https://doi.org/10.1111/j.1545-5300.1999.00143.x
11. T. L. Huston, J. P. Caughlin, R. M. Houts, S. E. Smith, L. J. George, The connubial crucible: Newlywed years as predictors of marital delight, distress, and divorce, *J. Pers. Soc. Psychol.*, **80** (2001), 237–252. https://doi.org/10.1037/0022-3514.80.2.237
12. B. R. Karney, T. N. Bradbury, The longitudinal course of marital quality and stability: A review of theory, methods, and research, *Psychol. Bull.*, **118** (1995), 3–34. https://doi.org/10.1037/0033-2909.118.1.3
13. C. E. Rusbult, C. Agnew, X. Arriaga, The Investment Model of Commitment Processes, in *Handbook of Theories of Social Psychology: Volume 2* (eds. P. Van Lange, A. Kruglanski and E. Higgins), SAGE Publications Ltd, (2012), 218–231. https://doi.org/10.4135/9781446249222.n37
14. J. M. Gottman, J. D. Murray, C. C. Swanson, R. Tyson, K. R. wanson, *The Mathematics of Marriage: Dynamic Nonlinear Models*, The MIT Press, 2002. https://doi.org/10.7551/mitpress/4499.001.0001
15. B. Barnes, I. Takyi, J. Ackora-Prah, G. Hughes, E. S. Baidoo, The mathematical model for marital interactions in Ghana, *Sci. Afr.*, **19** (2023), e01449. https://doi.org/10.1016/j.sciaf.2022.e01449
16. J. H. de la Cruz, J. M. Rey, A computational stochastic dynamic model to assess the risk of breakup in a romantic relationship, *Math. Methods Appl. Sci.*, **48** (2025), 7727–7744. https://doi.org/10.1002/mma.9292
17. J. Abreu-Afonso, M. M. Ramos, I. Queiroz-Garcia, I. Leal, How couple's relationship lasts over time? A model for marital satisfaction, *Psychol. Rep.*, **125** (2022), 1601–1627. https://doi.org/10.1177/00332941211000651
18. T. Y. Liu, H. X. Zhang, S. Wang, A new high-order compact CN-ADI scheme on graded meshes for three-dimensional nonlinear PIDEs with multiple weakly singular kernels, *Appl. Math. Lett.*, **171** (2025), 109697. https://doi.org/10.1016/j.aml.2025.109697
19. B. Øksendal, A. Sulem, *Applied Stochastic Control of Jump Diffusions*, Springer, Berlin, 2019. https://doi.org/10.1007/978-3-030-02781-0
20. S. Meyn, R. L. Tweedie, *Markov Chains and Stochastic Stability*, 2^{nd} edtion, Cambridge University Press, Cambridge, 2009. https://doi.org/10.1017/CBO9780511626630
21. P. Billingsley, *Convergence of Probability Measures*, Wiley Series in Probability and Statistics, 1999. https://doi.org/10.1002/9780470316962

22. D. Applebaum, *Lévy Processes and Stochastic Calculus*, 2nd edtion, Cambridge University Press, Cambridge, 2009. https://doi.org/10.1017/CBO9780511809781

AIMS Press